Minimizing Long-Term Energy Consumption in RIS-Assisted UAV-Enabled MEC Network

Zheng Yao, Qiwu Zhu, Yanhui Zhang, *Member, IEEE*, Haibo Huang, and Min Luo

***Abstract*—In recent years, Unmanned Aerial Vehicles (UAVs) are increasingly becoming flight-based communicative and computing platforms, but the scarcity of communication resources can significantly hinder their performance and scalability. Therefore, this paper proposes a Reconfigurable Intelligent Surface (RIS)-assisted UAV-enabled Mobile Edge Computing (MEC) network, that aims to reduce long-term energy consumption while maintaining system stability through jointly optimizing computing resources, time slot allocation, transmit power, RIS phase angles, and UAV trajectories. By applying the Lyapunov method, we transform the long-term stochastic optimization problem into manageable deterministic online subproblems, and obtain approximate optimal solutions using successive convex approximation, penalty functions, and convex optimization techniques. Simulation results show that compared to the baseline scheme, the proposed scheme approximately reduces energy consumption by 10%, improves system stability by approximately 16%, and maintains computational efficiency.**

***Index Terms*—Dynamic resource allocation, internet of things network, Lyapunov optimization, reconfigurable intelligent surface, succession convex approximation, unmanned aerial vehicle.**

I. Introduction

With the rapid advancement of Internet of Things (IoT) technology, an ever-increasing number of User Devices (UDs) and sensors are being connected to the network, forming a large-scale network for data generation and transmission [1]-[3]. The widespread application of IoT has driven a surge in data collection and processing demands, which means that efficient computing solutions and real-time responsiveness have become necessary. While traditional cloud computing architectures offer substantial processing power, their high latency and energy consumption make real-time data processing in IoT scenarios challenging [4]. Consequently, Mobile Edge Computing (MEC) has emerged as a solution, distributing computing resources closer to the data origin, effectively reducing transmission costs and enhancing system response speed and reliability.

Against this background, Unmanned Aerial Vehicles (UAVs) equipped with edge servers have aroused significant interest as a flexible and efficient MEC platform [5]-[7]. The UAVs can perform real-time data collection and processing by approaching the data sources, displaying unique advantages in scenarios like concerts, traffic jams, or earthquakes where base stations damaged or resources limited. This framework can operate in various complex ground environments, providing dynamic data processing capabilities [8], [9]. However, the main constraints for UAVs are battery life and energy management. Optimizing energy consumption while ensuring UAV performance remains a critical challenge.

Moreover, the massive access of wireless sensors has led to strained communication resources, prompting the introduction of Reconfigurable Intelligent Surface (RIS) technology as an innovative solution. The RIS can effectively improve communication quality by creating virtual links through signal reflection and by controlling the phase angles of these signals to achieve coherent superposition, thus significantly improving the channel quality and coverage [10]-[13]. As mentioned in reference [14], introducing the RIS technology in wireless communication network not only enhances the stability and reliability of wireless communication links, but also improves the communication efficiency of systems, effectively addressing challenges posed by scarce communication resources.

However, the introduction of RIS has brought new technological challenges to system optimization. Firstly, phase shift optimization itself is a high-dimensional complex variable non-convex problem, which is extremely complex; Secondly, the addition of RIS further exacerbates its coupling relationship with existing optimization variables and constraints in the system. These factors collectively led to a significant increase in optimization difficulty. For all that, references [15]-[18] have achieved significant achievements in optimizing the performance of RIS-assisted UAV-enabled MEC systems. Nevertheless, the most of existing research has primarily focused on the optimization of the instantaneous state of the system, with few efforts made to optimize the long-term system performance. In task-intensive scenarios, the tasks are not always processed on time. Therefore, long-term task queue management is crucial for efficient system operation, as it directly impacts data processing delays, resource allocation, and energy consumption optimization [19]. Especially in RIS-assisted UAV-enabled MEC systems, the communication capacity brought by RIS and the flexibility of UAV have led to the intensive offloading of tasks. If the queue is not effectively managed from a long-term perspective, it can lead to an overwhelming backlog of tasks that the system struggles to handle, and also render energy consumption control strategies inefficient. Furthermore, due to the explosive

This work was supported in part by the Hubei University of Automotive Technology PHD Initiation Fund under Grant 202404.

Zheng Yao, Haibo Huang, and Min Luo are with the School of Electrical and Information Engineering, Hubei University of Automotive Technology, Shiyan 442002, China (e-mail: yaozheng@huat.edu.cn; huang7855@163.com; 415656139@qq.com).

Qiwu Zhu is with the National Rail Transit Electrification and Automation Engineering Technology Research Center (Hong Kong Branch), Hong Kong Polytechnic University, Hongkong 999077, China (qi-wu.zhu@polyu.edu.hk).

Yanhui Zhang is with the Shenzhen Institute of Advanced Technology, Chinese Academy of Sciences, Shenzhen 517085, China (Zhangyh@siart.ac.cn).

growth of variable space caused by long-term optimization, how to significantly reduce the computational complexity of the algorithm while ensuring its accuracy has become a key challenge.

Based on the above discussion, this paper investigates minimizing energy consumption in the RIS-assisted UAV-enabled MEC system under long-term dynamic conditions, with a focus on the tradeoff between queue stability and system performance. The main contributions are outlined as follows.

1) ***Novel Network Architecture***: This paper considers a long-term RIS-assisted UAV-enabled MEC network model. Compared to existing works, we focus on the long-term performance of the system, aiming to achieve a tradeoff between system stability and minimizing long-term energy consumption by jointly optimizing computing resource, time slot ratio, transmit power, RIS phase angle, and UAV trajectory. To the best of our knowledge, this is a novel network architecture that is highly suitable for practical engineering applications.

2) ***Effective Problem Transformation***: To solve the proposed long-term stochastic optimization problem, based on the Lyapunov method, we approximately equivalently transform the original problem into a set of deterministic subproblems. Furthermore, a balance between system stability and performance is achieved through a weighting control factor, and the effectiveness of the transformation is conclusively demonstrated based on the theoretical analysis.

3) ***Low Complexity Algorithm Design***: Considering the coupling characteristics of variables between subproblems, we separately solve them based on alternating optimization. Firstly, based on convex optimization theory, we obtain an approximately optimal allocation of computing resources and time slot ratios with lower algorithm complexity. Additionally, the optimal RIS phase angle and transmit power are achieved by coherent accumulation of signals. Finally, to obtain the optimal UAV trajectory, we conduct a more thorough transformation of the problem based on the Successive Convex Approximation (SCA) method, acquiring the closed-form optimal solution for each iteration, and greatly reduce the algorithm complexity. The effectiveness of the proposed scheme is verified through simulations.

The remainder of this paper is structured as follows. Section II reviews related work. Section III presents our system model and problem formulation. In Section IV, we transform the problem based on Lyapunov theory. Section V details the problem solution, while Section VI provides a rigorous theoretical analysis of algorithm. Section VII presents our simulation results. Finally, Section VIII concludes the paper.

II. Related Work

With the maturity of RIS and UAV technology, more and more scholars are focusing on optimizing the performance of the RIS-assisted UAV-enabled MEC system. In recent years, research has primarily concentrated on utilizing the UAV as the airborne auxiliary base station, with a focus on optimizing the RIS phase angle, UAV trajectory, and resource allocation to enhance network performance. Qin et al. [20] considered both the amount of completed task bits and the energy consumption to maximize the energy efficiency of the RIS-assisted UAV-enabled MEC systems with non-orthogonal multiple access protocol. Moreover, deep reinforcement learning, as a universal approach, was used in [21]-[23] to optimize system performance. However, considering its poor generalization ability and time-consuming training, some scholars have explored using convex optimization or metaheuristic algorithms to replace it. Specifically, Mei et al. [24] aimed to maximize the energy efficiency of the RIS-assisted UAV-MEC system, they studied the joint optimization of UAV trajectory, task offloading, and cache with the phase-shift design of the RIS utilizing the SCA method. Meanwhile, Liao et al. [25] proposed a novel RIS-assisted UAV-MEC network architecture to support low-latency unmanned surface vehicles data computation with time window. Based on the Lagrangian relaxation method, alternating direction method of multipliers, and the SCA method, a heuristic solution was proposed to enhance task processing efficiency. Reference [26] maximized the computation capacity in a UAV-assisted MEC system equipped with RIS. Specifically, they respectively derived the optimal reflecting phase shift, resource allocation, decoding order, and the UAV deployment by invoking the concave-convex procedure method, the semidefinite relaxation technique, and the grid search method. Although the above work has achieved effective resource allocation and trajectory optimization in RIS-assisted UAV-enabled MEC system, their researches have been limited to an instantaneous state of system operation, without considering the stability of the system from a long-term perspective.

In practical engineering applications, optimizing performance while ensuring long-term system stability is very meaningful [27]. Firstly, the stable operation of the system is directly related to safety and efficiency. Secondly, continuous optimization makes the system more adaptable and resilient, enabling it to better respond to environmental changes. Recent advancements have seen extensive application of Lyapunov method in UAV-assisted MEC systems. This theoretical framework has demonstrated significant utility in enhancing system stability while approximating optimal operational efficiency [28]. Scholars have increasingly adopted this approach, exploring its potential to optimize the performance of modern wireless communications frameworks. In [29], Zeng et al. considered a UAV-assisted MEC system with a large service area, they transformed the original optimization problem into several deterministic subproblems based on the Lyapunov method, and solved these subproblems using convex optimization techniques, SCA methods, and alternating optimization. Zhang et al. [30] employed the Lyapunov optimization framework to dissect the problem of long-term energy consumption minimization in systems with task backlog queues. They segmented this overarching problem into three distinct online optimization subproblems, and a novel algorithm of reduced complexity was then developed to address these problems effectively. Meanwhile, the authors of [31] explored the optimization of a UAV-enabled MEC system serving multiple energy-harvesting devices. They aimed to develop an online algorithm that co-optimizes the energy usage and task processing rates of UAVs,

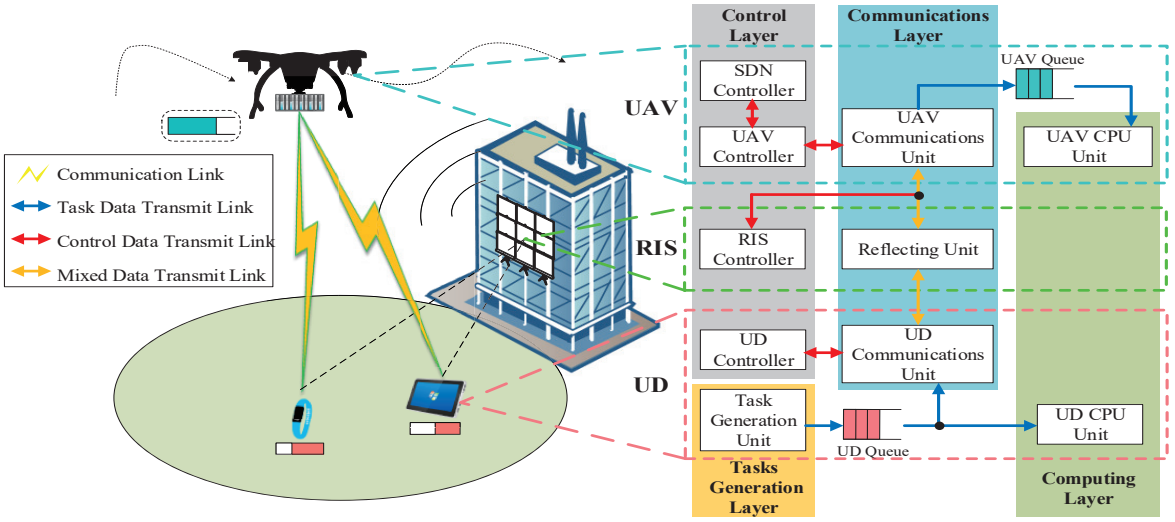

Fig. 1. RIS-assisted UAV-enabled MEC network system.

focusing on maintaining the stability of long-term data queues. The work of [32] tackled the challenge of minimizing the average weighted energy consumption across all users. The authors introduced two innovative strategies that sequentially address resource allocation and UAV trajectory planning to facilitate a balance between minimizing energy consumption and reducing queue backlog. Furthermore, in RIS-assisted UAV-enabled MEC system, Zhuo et al. [28] aimed to minimize energy consumption by considering various factors such as user transmission power, RIS phase shift, UAV trajectory, computational resource allocation, and the stability of queues. The above works have achieved effective results in long-term system optimization, but these algorithms used generally have high complexity. When the slot length is short, these solutions are unable to respond in a timely manner, greatly affecting the effectiveness of resource allocation and trajectory optimization.

Based on the existing challenges, this article aims to design an online low complexity resource allocation and trajectory optimization algorithm in a dynamic task intensive environment, in order to reduce long-term energy consumption while ensuring the stability of the RIS-assisted UAV-enabled MEC system.

III. System Model and Problem Formulation

In this section, we construct a RIS-assisted UAV-enabled MEC network model and present a long-term stochastic optimization problem. We formulate the communication model, the task and queue model, and the energy consumption model.

A. Overview

As shown in Fig. 1, we consider a RIS-assisted UAV-enabled MEC system, supported by software-defined network (SDN) technology. Specifically, this system consists of a UAV equipped with a MEC server, a passive RIS[1], and N UDs, the index set formed by all UDs is defined as $\boldsymbol{M} = \{1, 2, ..., m, ...,\mathrm{M}\}$. Meanwhile, each UD and UAV are equipped with a task buffer queue to cope with the impact of environmental fluctuations on the system. Therefore, the tasks of UDs can be offloaded to UAV and processed locally simultaneously. Moreover, we divide the continuous service time into discrete equidistant time slots to facilitate the online acquisition of allocation strategies. The set of slots can be represented as $\boldsymbol{N} = \{1, 2, ..., n, ...,\mathrm{N}\}$. Furthermore, the length of the time slot is δ_t, which is small enough to ensure that the quasi-static channel and the position of the UAV remain unchanged within each slot. Considering the function of system components, the constructed framework can include four layers: control layer, tasks generation layer, computing layer, and communication layer. The composition and function of these four-layer architectures will be detailed in the following.

- The control layer is implemented based on SDN. By virtualizing a centralized SDN controller in the MEC server, the decoupling of the system control link and data link is achieved. Specifically, the prior information of the system is first collected by the SDN controller (such as location coordinates, velocity, and queue status et al.), then feed into the optimization algorithm to obtain the reasonable dynamic resource allocation scheme. Finally, the control information is distributed to various components of the system for execution, thereby achieving effective utilization of system resources.
- The tasks generation layer is composed of all UDs. Each UD will generate some tasks during the duration of each slot. However, each UD only scans all tasks generated in the previous slot at the beginning of the current slot and accumulates them in the task buffer queue for allocation and processing. These tasks are usually fine-grained, can be divided in any proportion, and can be processed across slots to further improve resource utilization.
- The transmitter, receiver, and the RIS together form the communication layer, where both UDs and the UAV are equipped with transmitters and receivers to complete the task of offloading and downloading. It is worth noting that, similar to references [29] and [34], the impact of the downloading

[1]Compared to the passive RIS, active RIS can amplify the received signal through a built-in amplifier, effectively avoiding dual path fading effects. However, considering the impact of energy consumption constraint, thermal noise, hardware complexity and cost, this article introduces passive RIS to explore its impact on the long-term performance of the system. In future work, we will combine active RIS to acquire higher performance.

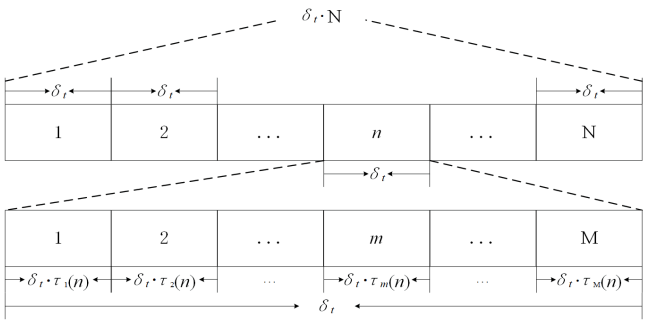

Fig. 2. The division model of sub-slot.

process on system stability and energy consumption is ignored, as the amount of feedback tasks is much smaller than the offloading process.

• The computing layer consists of CPUs from the UDs and MEC server. They retrieve the tasks that need to be processed from the buffer queues, compute them, and return the calculation results.

Based on the above introduction, after the task generation layer generates a task, it will be stored in the local queue and sending the status information to the control layer. The control layer monitors the system status in real-time and determines task and resource allocation strategies as needed, then the communication layer forwards these strategy instructions to various components for execution. For locally processed tasks, they can be directly sent from the local queue to the computing layer for processing. For tasks processed by the UAV, they are transmitted through the communication layer to the UAV queue and then sent to the computing layer for processing.

B. Communication Model

Compared to other wireless communication methods, the Time Division Multiple Access (TDMA) standard has some advantages, such as high-frequency spectrum utilization, strong anti-interference ability, and simple physical structure of the transceiver. Therefore, we utilize it to build offloading links. As shown in Fig. 2, each time slot is further divided into M sub-slots, and a UD independently occupies the channel to offload its task data in each sub-slot. It is worth noting that in order to further improve the utilization of time resources, the length of sub-slots occupied is adjustable. Meanwhile, the length of sub-slots occupied by the UD m in time slot n is defined as $\tau_m(n)$. Based on the above discussion and Shannon's theorem, the value of offloading data from UD m to the UAV in time slot n is as follows

$$D_m^o(n) = \tau_m(n) \cdot W \cdot \log_2(1 + \frac{P_m(n) \cdot |h_m(n)|^2}{W \cdot N_0}), \quad (1)$$

where W is the channel bandwidth, $P_m(n)$ represents the transmit power of UD m, $h_m(n) \in \mathbb{C}$ expresses the channel gain beteween UD m and the UAV in the slot n, and N_0 refers to the nosie power spectral density. Moreover, due to the length of the sub-slot is already small, the path gain in each sub-slot will not undergo significant changes.

For wireless communications, the channel gain $h_m(n)$ between the UAV and the UDs is a very significant factor, which can be regarded as the vector sum of two links: the direct link between the UAV and the UD, and the virtual link formed through the RIS. To provide a clearer description of the channel model, we introduced a Cartesian three-dimensional coordinate system. The location of ground UD m can be represented as $\boldsymbol{S}_m = \{x_m, y_m, 0\}$. Since the RIS is typically suspended on the surface of buildings with a fixed height H_R, its coordinate can be represented as $\boldsymbol{S}_R = \{x_R, y_R, H_R\}$. In addition, considering the mobility of the UAV, its position in n slot can be represented as $\boldsymbol{S}_U(n) = \{x_U(n), y_U(n), H_U\}$, where H_U is the hovering height. It is worth noting that RIS is composed of $M_R = M_x \times M_y$ reflective units, where M_x and M_y represent the number of reflective units of RIS in the horizontal direction and vertical direction, respectively. Meanwhile, considering the limited performance of UAV and UD, it is difficult to implement complex multi antenna beamforming technology. Therefore, both the UAV and the UDs adopt a single antenna configuration. Based on the above settings, we will provide a detailed introduction to the channel models of these two links separately in the following.

Firstly, we will introduce the channel gain of the direct link. Compared to high-altitude environments with only free space pathloss, due to obstacles such as buildings and trees, the low-altitude link between UAV and UDs may be often obstructed, resulting in a mixed environment of Line of Sight (LoS) and Non-Line of Sight (NLoS) links [35]. Note that the excessive path loss affecting the link largely depends on the propagation group composed of LoS and NLoS links. Therefore, we represent the expected excessive path loss as η_{NLoS} and η_{NLoS}, which is the additive average loss generated by low-altitude propagation over the free space path loss in high-altitude propagation. Furthermore, similarly as [36], the free space path loss between UD m and the UAV can be expressed as

$$h_m^f(n) = \sqrt{\frac{\beta_0}{d_m(n)^2}} e^{-j\frac{2\pi}{\lambda_r} d_m(n)}, \quad (2)$$

where β_0 refers to the unit path loss, $d_m(n) = \|\boldsymbol{S}_U(n) - \boldsymbol{S}_m\|_2$ expresses the distance between the UAV and UD m, and λ_r represents the wavelength of the carrier wave. Consequently, based on [35] and [36], the path gain model for the LoS and NLoS links are respectively represented as

$$h_m^{LoS}(n) = h_m^f(n)/\eta_{LoS}, \quad (3)$$

$$h_m^{NLoS}(n) = h_m^f(n) \cdot \Delta h_m^f(n)/\eta_{NLoS}, \quad (4)$$

where $\Delta h_m^f(n) \in \mathbb{C} \sim \mathcal{CN}(0,1)$ denotes the randomly scattered component of the channel experienced by UD m at time slot n. As described in [36], the probability of the LoS link between UD m and UAV at n slot is

$$P_m^{LoS}(n) = \frac{1}{1 + A \cdot e^{\{-B[\theta_m(n) - A]\}}}, \quad (5)$$

where A and B are coefficients influenced by the work environment, $\theta_m(n) = \frac{180}{\pi} \arcsin(H_U/d_m(n))$ is the elevation angle of UD m towards the UAV. Furthermore, the probability of NLoS link is $P_m^{NLoS}(n) = 1 - P_m^{LoS}(n)$. Accordingly, the average channel gain of the direct link is

$$h_m^d(n) = P_m^{LoS}(n) \cdot h_m^{LoS}(n) + P_m^{NLoS}(n) \cdot h_m^{NLoS}(n). \quad (6)$$

Furthermore, the virtual link can be further divided into two parts, namely the link between the UAV and RIS, and the link

between the RIS and UDs. The reflection angle matrix of RIS in the m sub-slot of the n slot can be written as

$$\boldsymbol{\Phi}_m(n) = \mathrm{diag}\big(e^{j\phi^m_{1,1}(n)}, ..., e^{j\phi^m_{m_x,m_y}(n)}, ..., e^{j\phi^m_{M_x,M_y}(n)}\big) \in \mathbb{C}^{M_R \times M_R}, \quad (7)$$

where $\phi^m_{m_x,m_y}(n) \in [0, 2\pi)$, $m_x \in \{1, 2, ..., M_x\}$, $m_y \in \{1, 2, ..., M_y\}$ represent the reflection phase angle of the m_x row and m_y column unit.

Considering that the link between the UAV and RIS is almost unobstructed, similar to literatures [37] and [38], the channel gain of this part can be formulated as

$$\begin{aligned}\boldsymbol{h}^u(n) =& \sqrt{\frac{\beta_0}{d^u(n)^2}} e^{-j\frac{2\pi}{\lambda_r} d^u(n)} \big[1, e^{-j\frac{2\pi\Delta x}{\lambda_r}\sin\theta^u(n)\cos\gamma^u(n)}, ..., \\ & e^{-j\frac{2\pi\Delta x}{\lambda_r}(M_x-1)\sin\theta^u(n)\cos\gamma^u(n)}\big] \\ & \otimes \big[1, e^{-j\frac{2\pi\Delta y}{\lambda_r}\sin\theta^u(n)\sin\gamma^u(n)}, ..., \\ & e^{-j\frac{2\pi\Delta y}{\lambda_r}(M_y-1)\sin\theta^u(n)\sin\gamma^u(n)}\big] \in \mathbb{C}^{M_R\times 1}, \end{aligned} \quad (8)$$

where $d^u(n) = \|\boldsymbol{S}_U(n) - \boldsymbol{S}_R\|_2$ is the distance between UAV and the suspension point of RIS, Δx and Δy respectively represent the spacing distance between each reflection unit in the horizontal and vertical directions, $\theta^u(n) = \frac{180}{\pi}\arcsin\left(|H_U - H_R|/d^u(n)\right)$ expresses the elevation angle of RIS towards the UAV, and $\gamma^u(n) = \frac{180}{\pi}\arctan\left(\frac{|x_U(n)-x_R|}{|y_U(n)-y_R|}\right)$ refers to horizontal angle between RIS and UAV.

Considering that there may be a small amount of obstruction between the UDs and the RIS, the link between them can be described through a Rician channel model. Hence, the Rician channel between the RIS and UD m is given by

$$\boldsymbol{h}^r_m(n) = \sqrt{\frac{\beta_0}{{d^r_m}^2}}\left[\sqrt{\frac{\kappa_r}{1+\kappa_r}}\boldsymbol{h}^{r,LoS}_m + \sqrt{\frac{1}{1+\kappa_r}}\Delta\boldsymbol{h}^r_m(n)\right], \quad (9)$$

where $\Delta\boldsymbol{h}^r_m(n) \in \mathbb{C}^{M_R\times 1} \sim \mathcal{CN}(0, \mathbf{I}_{M_R})$ is the randomly scattered component, κ_r represents the randomly scattered component, and the LoS component $\boldsymbol{h}^{r,LoS}_m$ can be obtain as

$$\begin{aligned}\boldsymbol{h}^{r,LoS}_m =& e^{-j\frac{2\pi}{\lambda_r}d^r_m}\big[1, e^{-j\frac{2\pi\Delta x}{\lambda_r}\sin\theta^r_m\cos\gamma^r_m}, ..., \\ & e^{-j\frac{2\pi\Delta x}{\lambda_r}(M_x-1)\sin\theta^r_m\cos\gamma^r_m}\big] \\ & \otimes \big[1, e^{-j\frac{2\pi\Delta y}{\lambda_r}\sin\theta^r_m\sin\gamma^r_m}, ..., \\ & e^{-j\frac{2\pi\Delta y}{\lambda_r}(M_y-1)\sin\theta^r_m\sin\gamma^r_m}\big] \in \mathbb{C}^{M_R\times 1}, \end{aligned} \quad (10)$$

where d^r_m is the distance between RIS and UD m, $\theta^r_m = \frac{180}{\pi}\arcsin\left(H_R/d^r_m\right)$ expresses the elevation angle of UD m towards the RIS, and $\gamma^r_m = \frac{180}{\pi}\arctan\left(\frac{|x_R-x_m|}{|y_R-y_m|}\right)$ refers to horizontal angle between UD m and RIS.

Based on the above introduction of the two parts, the channel gain of the virtual link can be expressed as

$$h^v_m(n) = \big(\boldsymbol{h}^r_m(n)\big)^H \boldsymbol{\Phi}_m(n)\boldsymbol{h}^u(n) \in \mathbb{C}. \quad (11)$$

Consequently, through vector combining the channel gains of the direct link and the virtual link, the channel gain between UD m and the UAV can be obtained as

$$h_m(n) = h^d_m(n) + h^v_m(n). \quad (12)$$

C. Task and Queue Model

In the proposed system, both the UAV and the UDs are equipped with the task buffer queue. Meanwhile, assuming that each UD generates some tasks during each time slot. However, considering that the device's perception of the environment and its state is intermittent, these tasks will be detected at the beginning of the next slot and merged into a large data packet. Denote this data packet by the tuple $\zeta_m(n) \triangleq \{A_m(n), \varphi\}$, where $A_m(n)$ is the size of the task, φ denotes the required CPU cycles to process 1bit data. Supposing that $A_m(n)$ is independent and identically distributed in each slot with the Poisson distribution and $\mathbb{E}\{A_m(n)\} = \lambda, m \in \boldsymbol{M}$. The tasks will first be cached in the UDs' queue, then retrieved for local processing or offloaded to the UAV for further execution. Similarly, the offloaded tasks will first be cached in the queue of the UAV and then processed sequentially by the MEC server. Both of these queues adopt the first-in-first-out order.

Specifically, to further improve the utilization of system resources, we have adopted dynamic voltage regulation technology, which means that the processing frequency of UDs and UAV can be controlled and varied. Define the processing frequency of UD m and the UAV as $f_m(n)$ and $f_u(n)$, respectively. In each time slot, the size of the processed tasks of UD m locally and MEC is determined by the following equation [39]

$$D_m(n) = \frac{f_m(n)\delta_t}{\varphi}, \quad (13)$$

$$D_u(n) = \frac{f_u(n)\delta_t}{\varphi}. \quad (14)$$

Based on the above model of tasks, we will further introduce the update process of the queues. Define $Q_m(n)$ and $L(n)$ as the length of the queues for UD m and the UAV in the n-th slot, respectively. Note that tasks processed in the previous time slot will be directly retrieved from the buffer queue, while newly arrived tasks will need to wait for detection in the next time slot. Consequently, the update process of $Q_m(n)$ and $L(n)$ are obtained as follows:

$$Q_m(n+1) = [Q_m(n) - D_m(n) - D^o_m(n)]^+ + A_m(n), \quad (15)$$

$$L(n+1) = [L(n) - D_u(n)]^+ + \sum\nolimits_{m\in\boldsymbol{M}} D^o_m(n), \quad (16)$$

where $[x]^+ \triangleq \max\{x, 0\}$.

D. Energy Consumption Model

In the proposed system, the energy consumption of system mainly includes three aspects: offloading energy consumption, computing energy consumption, and flying consumption.

1) Computing Energy Consumption

Similar to references [13] and [40], we assume that the computing energy consumption of both UAV and UDs is mainly influenced by the frequency of computation, which can be expressed as

$$e_m(n) = \kappa_c \cdot f_m(n)^3 \cdot \delta_t, \quad (17)$$

$$e_u(n) = \kappa_c \cdot f_u(n)^3 \cdot \delta_t, \quad (18)$$

where κ_c is the capacitance architecture coefficient of the CPU, and the CPUs of the same model have the same κ_c.

2) Transmit Energy Consumption

Considering that UD m in each slot can only transmit tasks in the allocated sub-slot, while the transmitter is in sleep mode at other times. Therefore, the transmission energy consumption of UD m can be expressed as

$$e_m^p(n) = P_m(n) \cdot \tau_m(n). \tag{19}$$

3) Flying Energy Consumption

Due to the short length of each time slot, it is reasonable to assume that the UAV performs uniform straight-line flight within one time slot. Based on this assumption, as described in reference [37] and [40], define the flying speed of UAV as $v(n) = \|\boldsymbol{S}_U(n) - \boldsymbol{S}_U(n-1)\|_2/\delta_t$, and the flying energy consumption of UAV can be obtained as follows

$$\begin{aligned} e_f(n) =& \delta_t P_o \left(1 + \frac{3v(n)^2}{\Omega^2 {r_f}^2}\right) + \frac{\delta_t P_i v_0}{v(n)^2} \\ &+ \frac{1}{2}\delta_t d_0 \rho_f s_f A_r v(n)^3, \end{aligned} \tag{20}$$

where P_o and P_i are the blade profile power and induced power in hovering status, Ω expresses the blade angular velocity, r_f represents the rotor radius, v_0 refers to the induced velocity for rotor in forwarding flight, d_0 is the fuselage drag ratio, ρ_f denotes the air density, s_f means the rotor solidity, and A_r expresses the rotor disc area.

E. Problem Formulation

In the IoT network, both the UAV and UDs are powered by batteries, which makes them very sensitive to energy consumption. Moreover, considering that the proposed system is a long-term operation, its stability is also very important and is related to its normal operating state. Therefore, we propose a long-term stochastic optimization problem to minimize long-term energy consumption under system stability, through jointly optimizing computing frequency, sub-slot allocation, phase angle control, and flying trajectories. Furthermore, in order to research the ultimate performance of the system, we set N to infinity ($\mathrm{N} \to \infty$), which can obtain the theoretical boundaries of system performance. Subsequently, the optimization problem can be expressed as

$$\begin{aligned} P1: \min_{\boldsymbol{\zeta}(n)} \quad & \lim_{\mathrm{N}\to\infty} \frac{1}{\mathrm{N}} \sum\nolimits_{n\in\boldsymbol{N}} \Big\{ e_u(n) + \varepsilon e_f(n) \\ & + \sum\nolimits_{m\in\boldsymbol{M}} \big\{ e_m(n) + e_m^p(n) \big\} \Big\} && \text{(21a)} \\ \text{s.t.} \quad & C1: 0 \le f_m(n) \le F_{max}^l, && \text{(21b)} \\ & C2: 0 \le f_u(n) \le F_{max}^u, && \text{(21c)} \\ & C3: 0 \le \tau_m(n), && \text{(21d)} \\ & C4: \sum\nolimits_{m\in\boldsymbol{M}} \tau_m(n) \le \delta_t, && \text{(21e)} \\ & C5: 0 \le \phi_{m_x,m_y}^m(n) < 2\pi, && \text{(21f)} \\ & C6: 0 \le P_m(n) \le P_{max}, && \text{(21g)} \\ & C7: v(n) \le v_{max}, && \text{(21h)} \\ & C8: \boldsymbol{S}_u(1) = \boldsymbol{S}_I, \boldsymbol{S}_u(\mathrm{N}) = \boldsymbol{S}_F, && \text{(21i)} \\ & C9: \lim_{\mathrm{N}\to\infty} \frac{1}{\mathrm{N}} \sum\nolimits_{n\in\boldsymbol{N}} \mathbb{E}\{Q_m(n)\} < \infty, && \text{(21j)} \\ & C10: \lim_{\mathrm{N}\to\infty} \frac{1}{\mathrm{N}} \sum\nolimits_{n\in\boldsymbol{N}} \mathbb{E}\{L(n)\} < \infty, && \text{(21k)} \end{aligned}$$

where $\boldsymbol{\zeta}(n) \triangleq \{\boldsymbol{F}(n),\ f_u(n),\ \boldsymbol{\tau}(n),\ \boldsymbol{\Psi}(n),\ \boldsymbol{P}(n),\ \boldsymbol{S}_U(n)\}$ represents the set of optimization variables, $\boldsymbol{F}(n) \triangleq \{f_1(n), f_2(n), ..., f_{\mathrm{M}}(n)\} \in \mathbb{R}^{\mathrm{M}\times 1}$ denotes the set of UDs' computing frequency, $\boldsymbol{\tau}(n) \triangleq \{\tau_1(n), \tau_2(n), ..., \tau_{\mathrm{M}}(n)\} \in \mathbb{R}^{\mathrm{M}\times 1}$ expresses the set of sub-slot allocation, $\boldsymbol{\Psi}(n) \triangleq \{\boldsymbol{\Phi}_1(n), \boldsymbol{\Phi}_2(n), ..., \boldsymbol{\Phi}_{\mathrm{M}}(n)\} \in \mathbb{C}^{\mathrm{M}\times M_R\times M_R}$ is the set of phase angle controls for all sub-slots under n slot, $\boldsymbol{P}(n) \triangleq \{P_1(n), P_2(n), ..., P_{\mathrm{M}}(n)\}$ refers to the set of transmit power, ε refers to the attenuation factor of flying energy consumption, F_{max}^l and F_{max}^u represent the maximum computing frequency of UDs and the UAV, P_{max} expresses the maximum power of UD transmitter, v_{max} is defined as the maximum speed of the UAV, $\boldsymbol{S}_I$ and $\boldsymbol{S}_F$ are the initial and final points, respectively. Furthermore, $C1$ and $C2$ ensure that the computing frequency of UDs and UAV do not exceed their physical limitations; $C3$ and $C4$ guarantee that the sum of sub-slots is not more than the length of the slot; $C5$ expresses the range of phase angle regulation for reflective units; $C6$ is the working range constraint of the transmitter; $C7$ specifies the upper limit of flying speed; $C8$ has set the takeoff and landing positions of the UAV; $C9$ and $C10$ guarantee the stability of queues, which means that the queues lengths remain finite and do not scale up to infinite over time.

The incorporation of constraints $C9$ and $C10$ significantly enhances the stability of the proposed system, ensuring an exemplary experience for all modules. Nevertheless, the complexity of addressing the problem is compounded by these constraints, especially considering the objective function's focus on long-term optimization. In addition, unlike maximizing the data rate in reference [11], simply maximizing the data rate can certainly make constraint $C9$ strong, but it will consume more energy and may make $C10$ unsatisfied. Therefore, we need to optimize resource allocation to find suitable data rates and offloading decisions, and strike a balance between energy loss and system stability. This introduces considerable challenges in solution derivation.

IV. Problem Transformation

The application of the Lyapunov optimization method in stochastic networks is primarily due to its ability to ensure system stability and address intricate optimization challenges. This method outperform other methods, like metaheuristic algorithms, because it operates without the need for statistical data from associated stochastic models, relying solely on immediate queue backlog data to guide control decisions. Additionally, in the long-term optimization problem, the continuous expansion of the policy space leads to a significant decrease of the metaheuristic algorithm performance. However, Lyapunov optimization method transforms long-term optimization problem into manageable online scheduling problem. This shift simplifies the problem by separating it from temporal constraints, significantly reducing computational complexity and facilitating practical implementation. Consequently, this section presents the development of an adaptable and robust algorithm leveraging Lyapunov theory. Drawing on approaches from the literature [29] and [41], we reformulate the original problem $P1$ into a deterministic online optimization challenge

at each time slot using Lyapunov technique. The specifics of our approach begin with the establishment of a quadratic Lyapunov function.

$$V(n) = \frac{\sum_{m\in \boldsymbol{M}} Q_m(n)^2}{2} + \frac{L(n)^2}{2}. \tag{22}$$

Next, we define the conditional Lyapunov drift function $\Delta V(n)$ to evaluate changes between two successive time slots.

$$\Delta V(n) = \mathbb{E}\{V(n+1) - V(n)|\boldsymbol{\mathcal{Q}}(n)\}, \tag{23}$$

where $\boldsymbol{\mathcal{Q}}(n) \triangleq \{Q_1(n), Q_2(n), ..., Q_{\mathrm{M}}(n), L(n)\}$ is the set of system buffer queue in n-th slot. Similar to references [29] and [30], we introduce the Lyapunov control factor $V_L \geq 0$, which facilitates a tradeoff between minimizing energy consumption and maintaining system stability. Consequently, enhancing the predictability and efficiency of system operations, the Lyapunov drift-plus-penalty function is formulated to quantify this equilibrium, which can be shown as follows

$$\begin{aligned}\mathcal{D}(n) =& V_L\mathbb{E}\Big\{e_u(n)+\varepsilon e_f(n)+\sum_{m\in \boldsymbol{M}}\big\{e_m(n)+e_m^p(n)\big\}\Big|\boldsymbol{\mathcal{Q}}(n)\Big\}\\ &+\Delta V(n).\end{aligned} \tag{24}$$

The Lyapunov drift function is often complex due to the evolution of the system's state, and optimizing it typically involves solving intricate dynamic equations or requires knowledge of future system states. Therefore, directly optimizing the drift-plus-penalty is often impractical or challenging in real-world scenarios. Hence, we will optimize the upper bound of the drift-plus-penalty to achieve the tradeoff. Although we have changed the goal form, the appropriate selection and design of this upper bound can still ensure system stability and performance. This approach has been proven effective in numerous works (e.g., [28] and [42]), and the feasibility of this proposal will also be verified in the subsequent chapter. Subsequently, the upper bound of drift-plus-penalty is introduced as follows.

To scale the Lyapunov function, two inequalities are first introduced, namely given $X > 0$, $Y > 0$, and $Z > 0$, the following formulas always hold

$$\{[X-Y]^+ + Z\}^2 - X^2 \leq Y^2 + Z^2 + 2X(Z-Y), \tag{25}$$

$$\begin{aligned}&\Big\{[X+\sum_{i=1}^{Y} Y_i]^+ + \sum_{j=1}^{Z} Z_j\Big\}^2 - X^2 \leq \sum_{i=1}^{Y}(X+Y_i)^2\\ &\quad+\sum_{j=1}^{Z}(X+Z_j)^2 - (Y+Z)X^2 + \Big\{\sum_{i=1}^{Y} Y_i + \sum_{j=1}^{Z} Z_j\Big\}^2.\end{aligned} \tag{26}$$

Based on the (15) and (25), we can obtain

$$\begin{aligned}&Q_m(n+1)^2 - Q_m(n)^2\\ =&\{[Q_m(n) - D_m(n) - D_m^o(n)]^+ + A_m(n)\}^2 - Q_m(n)^2\\ \leq& A_m(n)^2 + 2Q_m(n)A_m(n) + [D_m(n) + D_m^o(n)]^2\\ &- 2Q_m(n)[D_m(n) + D_m^o(n)].\end{aligned} \tag{27}$$

Meanwhile, based on the (16) and (26), it is possible to derive

$$\begin{aligned}&L(n+1)^2 - L(n)^2\\ =&\Big\{[L(n) - D_u(n)]^+ + \sum_{m\in \boldsymbol{M}} D_m^o(n)\Big\}^2 - L(n)^2\\ \leq& [L(n) - D_u(n)]^2 + \sum_{m\in \boldsymbol{M}}\big[L(n) + D_m^o(n)\big]^2\\ &- (\mathrm{M}+1)L(n)^2 + \big[-D_u(n) + \sum\nolimits_{m\in \boldsymbol{M}} D_m^o(n)\big]^2\\ \leq& \sum_{m\in \boldsymbol{M}}\Big\{2D_m^o(n)^2 + 2[L(n) - D_u(n)]D_m^o(n)\Big\}\\ &+ 2D_u(n)^2 - 2L(n)D_u(n).\end{aligned} \tag{28}$$

Based on the formulation of the Lyapunov drift-plus-penalty function as outlined in equation (24), and substituting (27) and (28) into it, we can obtain

$$\begin{aligned}&\mathcal{D}(n)\\ &= \mathbb{E}\Big\{V_L\Big[e_u(n) + \varepsilon e_f(n) + \sum_{m\in \boldsymbol{M}}\big\{e_m(n) + e_m^p(n)\big\}\Big]\\ &\quad+\frac{L(n+1)^2 - L(n)^2}{2} + \sum_{m\in \boldsymbol{M}}\frac{Q_m(n+1)^2 - Q_m(n)^2}{2}\Big|\boldsymbol{\mathcal{Q}}(n)\Big\}\\ &\leq \mathbb{E}\Big\{C^1(n) + V_L\Big[e_u(n) + \varepsilon e_f(n) + \sum_{m\in \boldsymbol{M}}\big\{e_m(n) + e_m^p(n)\big\}\Big]\\ &\quad+\sum_{m\in \boldsymbol{M}}\Big\{D_m^o(n)^2 + [L(n) - D_u(n)]D_m^o(n)\Big\} + D_u(n)^2\\ &\quad- L(n)D_u(n) - \sum_{m\in \boldsymbol{M}}\Big\{Q_m(n)[D_m(n) + D_m^o(n)]\\ &\quad-\frac{[D_m(n)+D_m^o(n)]^2}{2}\Big\}\Big|\boldsymbol{\mathcal{Q}}(n)\Big\},\end{aligned} \tag{29}$$

where $C^1(n) = \sum_{m\in \boldsymbol{M}}\{A_m(n)^2/2 + Q_m(n)A_m(n)\}$ represents a constant. Base on (29), by eliminating terms that do not depend on the optimization variables, and organizing these terms, we can reformulate problem $P1$ into an equivalent optimization problem, designated as $P2$, listed as follows:

$$\begin{aligned}P2: \min_{\boldsymbol{\zeta}(n)} &\sum_{m\in \boldsymbol{M}}\Big\{V_L\big[e_m(n) + e_m^p(n)\big] + \frac{3D_m^o(n)^2 + D_m(n)^2}{2}\\ &+[L(n) - D_u(n) - Q_m(n) + D_m(n)]D_m^o(n)\\ &- Q_m(n)D_m(n)\Big\} + V_L e_u(n) + V_L\varepsilon e_f(n)\\ &+ D_u(n)^2 - L(n)D_u(n)\\ \text{s.t.}\quad & C1 - C8.\end{aligned} \tag{30}$$

It is worth noting that the constraints $C9$ and $C10$ have $P2$, and the long-term stochastic optimization problem also has been transformed into an online deterministic optimization problem. This transformation is approximately equivalent, and in order to demonstrate its effectiveness, we have conducted a detailed derivation of the theoretical gap between them in section VI.

V. Problem Solution

Due to the intricate coupling among optimization variables in problem P2, we decomposed it into three sub-optimization

problems. To tackle these effectively, we developed an online algorithm using an alternating optimization strategy to approximate the optimal solution of the original problem. This approach involves iteratively finding optimal solutions for each subproblem while keeping other variables fixed, and repeating this process until the change in the objective function is less than σ_A.

Moreover, to address the potential surge in algorithmic complexity brought about by the alternating optimization, we derived closed-form solutions for the subproblems or approximated them using algorithms of notably low complexity. This strategy ensures efficiency and feasibility in implementation. In the following sections, we will elaborate on the methodologies employed to solve these subproblems.

A. Computing Resource Allocation

Through fixed time slot allocation, reflection angle, and UAV trajectory, problem $P2$ is only affected by the UAV and UDs computing frequencies. Considering that there is no coupling between these two optimization variables, they can be solved separately. Specifically, by extracting the items in problem $P2$ that are only related to the computing frequency of the UAV, the following problem can be obtained

$$\begin{aligned} SP1: \min_{f_u(n)} & \Big[\frac{f_u(n)\delta_t}{\varphi}\Big]^2 - \Big[L(n) + \sum_{m\in \boldsymbol{M}} D_m^o(n)\Big]\frac{f_u(n)\delta_t}{\varphi} \\ & + V_L\kappa_c f_u(n)^3\delta_t \\ \text{s.t.} \quad & 0 \le f_u(n) \le F_{max}^u. \end{aligned} \tag{31}$$

Sub-problem $SP1$ is a straightforward convex optimization problem. By taking the partial derivative of its objective function and setting it equal to zero, we can derive the optimal solution.

$$f_u(n)' = \frac{\sqrt{\frac{{\delta_t}^2}{\varphi^4} + 3V_L\kappa_c[L(n) + \sum_{m\in\mathcal{M}} D_m^o(n)]/\varphi} - \frac{{\delta_t}^2}{\varphi^2}}{3V_L\kappa_c}. \tag{32}$$

Considering the influence of constraints, with the given transmission data $D_m^o(n)$, the optimal computing frequency of UAV can be obtained

$$f_u(n)^* = \begin{cases} 0, & f_u(n)' < 0, & \text{(33a)} \\ f_u(n)', & 0 \le f_u(n)' \le F_{max}^u, & \text{(33b)} \\ F_{max}^u, & F_{max}^u < f_u(n)'. & \text{(33c)} \end{cases}$$

Similarly, the sub-problem of local computing frequency is

$$\begin{aligned} SP2: \min_{\boldsymbol{F}(n)} & \sum_{m\in\boldsymbol{M}} \Big\{V_L\kappa_c f_m(n)^3\delta_t - [Q_m(n) + D_m^o(n)]\frac{f_m(n)\delta_t}{\varphi} \\ & + \frac{f_m(n)^2{\delta_t}^2}{2\varphi^2}\Big\} \\ \text{s.t.} \quad & 0 \le f_m(n) \le F_{max}^m. \end{aligned} \tag{34}$$

The sub-problem $SP2$ is also a simple convex optimization problem, and its closed-form solution can be obtained using the method of solving problem $SP1$. Due to space constraints, further details will not be elaborated here.

B. Time Slot Ratio Allocation

Under fixed computing frequency, reflection angle, and UAV trajectory, this section focuses on optimizing the length of time slot allocated to each UD. Specifically, we isolate the terms related to time slot allocation $\tau_m(n)$ from problem $P2$ to obtain the sub-problem $SP3$ listed as follows:

$$\begin{aligned} SP3: \min_{\boldsymbol{\tau}(n)} & \sum_{m\in\boldsymbol{M}} \Big\{\frac{3}{2}[r_m(n)\cdot\tau_m(n)]^2 + V_L P_m(n)\tau_m(n) \\ & + C_m^2(n) r_m(n)\tau_m(n)\Big\} \\ \text{s.t.} \quad & 0 \le \tau_m(n), \\ & \sum_{m\in\boldsymbol{M}} \tau_m(n) \le \delta_t, \end{aligned} \tag{35}$$

where $r_m(n) = W\cdot\log_2(1 + \frac{p_m\cdot|h_m(n)|^2}{W\cdot N_0})$ and $C_m^2(n) = [L(n) - D_u(n) - Q_m(n) + D_m(n)]$ are constants value. Mathematically, the sub-problem $SP3$ also is a convex problem. Due to the coupling relationship between time slot allocation strategies among different UDs, the solution to this sub-problem becomes challenging. However, the sub-problem $SP3$ is a convex problem with 0 dual gap. Therefore, we design a low-complexity algorithm based on Lagrange duality and Karush-Kuhn-Tucker condition. Firstly, define the Lagrange function for problem $SP3$ as

$$\begin{aligned} \mathcal{L}(\boldsymbol{\tau}(n), \boldsymbol{\alpha}, \beta) = & \sum_{m\in\boldsymbol{M}} \Big\{\frac{3}{2} r_m(n)^2\tau_m(n)^2 + V_L P_m(n)\tau_m(n) \\ & + C_m^2(n) r_m(n)\tau_m(n)\Big\} - \sum_{m\in\boldsymbol{M}} \alpha_m\tau_m(n) \\ & + \beta\Big\{\sum_{m\in\boldsymbol{M}} \tau_m(n) - \delta_t\Big\}, \end{aligned} \tag{36}$$

where $\alpha_m \ge 0$ and $\beta \ge 0$ represent the Lagrange multipliers corresponding to constraint $C3$ and $C4$ respectively, and $\boldsymbol{\alpha} \triangleq \{\alpha_1, \alpha_2, ..., \alpha_{\mathrm{M}}\}$ encapsulates the set of multipliers for the constraint $C3$. Under the Karush-Kuhn-Tucker condition, specific equations must be satisfied to determine the optimal slot ratio ${\tau_m}^*(n)$. These equations ensure that the solution adheres to the constraints and optimality criteria of the underlying optimization problem.

$$\begin{cases} 3r_m(n)^2{\tau_m}^*(n) + V_L P_m(n) \\ \qquad + C_m^2(n) r_m(n) - {\alpha_m}^* + \beta^* = 0, & \text{(37a)} \\ {\alpha_m}^*{\tau_m}^*(n) = 0, & \text{(37b)} \\ \beta^*\Big\{\sum_{m\in\boldsymbol{M}} {\tau_m}^*(n) - \delta_t\Big\} = 0, & \text{(37c)} \\ {\tau_m}^*(n) \ge 0, & \text{(37d)} \\ \sum_{m\in\boldsymbol{M}} {\tau_m}^*(n) \le \delta_t, & \text{(37e)} \\ {\alpha_m}^* \ge 0, \beta^* \ge 0. & \text{(37f)} \end{cases}$$

By conducting straightforward algebraic manipulations on equation (37a), we can derive the expression for the optimal slot ratio ${\tau_m}^*(n)$, as follows:

$${\tau_m}^*(n) = \frac{{\alpha_m}^* - \beta^* - V_L P_m(n)}{3r_m(n)^2} - \frac{C_m^2(n)}{3r_m(n)}. \tag{38}$$

After substituting the expression from (38) into equation (37b), we can derive the resulting equation as follows:

$${\alpha_m}^*\Big\{\frac{{\alpha_m}^* - \beta^* - V_L P_m(n)}{3r_m(n)^2} - \frac{C_m^2(n)}{3r_m(n)}\Big\} = 0. \tag{39}$$

Obviously, equation (39) presents two distinct solutions for ${\alpha_m}^*$. One solution is ${\alpha_m}^* = 0$, and the other refers to ${\alpha_m}^* = C_m^2(n) r_m(n) + \lambda^*$. Based on these two solutions, according to formula (38), two optimal slot ratios can be obtained, namely

$$\begin{cases} {\tau_m}^*(n) = 0, & \text{(40a)} \\ {\tau_m}^*(n) = \dfrac{C_m^2(n)}{3r_m(n)} - \dfrac{\beta^* + V_L P_m(n)}{3r_m(n)^2}, & \text{(40b)} \end{cases}$$

where the second item is only related to another Lagrange multiplier β^*. It is worth noting that, when $C_m^2(n) < 0$, regardless of the value of β^*, ${\tau_m}^*(n)$ will always be less than 0, which clearly contradicts equation (36d). Therefore, when $C_m^2(n) < 0$, ${\tau_m}^*(n) = 0$. This can also be inferred from the objective function of *SP*3, when $C_m^2(n) < 0$, the objective function is monotonically increasing. To minimize it as much as possible, the optimal time slot ratio for the UD m should be set to 0.

Given that both potential solutions from equation (39) satisfy the equation, the solution that minimizes the objective function should be selected under the chosen β^*. To this end, a variable speed binary search method is utilized to closely approximate the optimal β^* and, consequently, the nearly optimal time slot ratio. Specifically, given an initial value of $\beta = 0$, substitute it into (39) and calculate the objective function of UD m under two different slot ratios, as detailed in (40a) and (40b), respectively, as well as the lower of the two objective function values should be selected. This process is repeated across all UDs to establish the best strategy for each under the given β. The results are then aggregated to compute the total slot ratio. According to (38), the value of $\tau_m(n)$ monotonically decreases with an increase in β. Accordingly, if the total slot ratio is greater than δ_t, β should be increased; otherwise, β should be decreased. To improve the efficiency of the search, we use a relatively large fixed step size Δ_τ when increasing the β. When the sum value is less than Δ_τ for the first time, we use the binary method for fine search. In addition, when the change of the objective function during the iterative search process is less than σ_τ, it is considered that the approximation has reached the optimum, and the iterative process is halted. The specific procedural steps are outlined in the Algorithm 1, ensuring a systematic and efficient search for the optimal parameters.

C. Phase Angle and Transmit Power Optimization

In this section, we will jointly optimize the phase angle and transmit power. Similar to the previous operation, by isolating the terms related to both variables in problem $P2$, we can formulate the sub-optimization problem $SP4$.

$$\begin{aligned} SP4: \min_{\boldsymbol{\Psi}(n), \boldsymbol{P}(n)} \sum_{m \in \boldsymbol{M}} \Big\{ & V_L \tau_m(n) P_m(n) + \frac{3}{2} D_m^o(n)^2 \\ & + C_m^2(n) D_m^o(n) \Big\} \\ \text{s.t.} \quad & C5, C6. \end{aligned} \tag{41}$$

To solve problem $SP4$, we first give the following proposition.

Proposition 1. *The optimal solution to $SP4$ can be achieved if and only if the best channel gain is obtained by adjusting coefficient matrix $\boldsymbol{\Psi}(n)$.*

Algorithm 1 Time slot ratio optimization algorithm.

Initialization: $r_m(n)$, $L(n)$, $D_u(n)$, $Q_m(n)$, $D_m(n)$, δ_t, Δ_τ, σ_τ, $k = 0$, $\beta_1 = 0$, and $I_\tau = 0$.
while 1 **do**
  $k = k + 1$;
  for n = 1:N **do**
    if $D_u(n) - L(n) + Q_m(n) - D_m(n) < 0$ **then**
      ${\tau_m}^* = 0$;
    else
      Calculate two different time slot ratios based on formulas (40a) and (40b);
      Substitute the ratio of two slots into the objective function of (35), and denote the corresponding ratio as ${\tau_m}^*$ if it is smaller, and its objective function is U_m^k;
    end if
  end for
  if $|\sum_{m \in \boldsymbol{M}} U_m^k - \sum_{m \in \boldsymbol{M}} U_m^{k-1}| < \sigma_\tau$ **then**
    Break;
  end if
  Sum up the time slot ratios of all UDs to obtain τ_{sum};
  if $\tau_{sum} > \delta_t$ and $I_\tau = 0$ **then**
    $\beta_{k+1} = \beta_k + \Delta_\tau$;
  else
    $I_\tau = 1$;
    if $\tau_{sum} = \delta_t$ **then**
      $\beta_{k+1} = \beta_k$;
    else
      if $\tau_{sum} < \delta_t$ **then**
        $\beta_{k+1} = \beta_k - \frac{|\beta_k - \beta_{k-1}|}{2}$;
      else
        $\beta_{k+1} = \beta_k + \frac{|\beta_k - \beta_{k-1}|}{2}$;
      end if
    end if
  end if
end while
Output the optimal time slot ratios $\boldsymbol{\tau}(n)$.

Proof. Firstly, assuming that $\{\boldsymbol{\Psi}(n)^*, \boldsymbol{P}(n)^*\}$ is the optimal solutions of $SP4$, while the channel gain $h_m(n)^*$ induced by $\boldsymbol{\Psi}(n)^*$ is not best, then there exists $\boldsymbol{\Psi}(n)'$ leading to a better channel gain $h_m(n)'$. Subsequently, we can create a new solution that meets $P_m(n)' = \frac{h_m(n)^*}{h_m(n)'} P_m(n)^* < P_m(n)^*$. Obviously, the transmission rates corresponding to the two solutions are the same. Considering when $P_m(n)' < P_m(n)^*$, the value of objective function in $SP4$ based on $\{\boldsymbol{\Psi}(n)', \boldsymbol{P}(n)'\}$ is smaller than the objective function value corresponding to $\{\boldsymbol{\Psi}(n)^*, \boldsymbol{P}(n)^*\}$, which contradicts the assumption. Therefore, the optimal phase shifts $\boldsymbol{\Psi}(n)$ in $SP4$ will definitely lead to the best channel gain. □

Based on **Proposition 1**, the optimization problem regarding the phase angle can be reformulated as a channel gain maximization problem, which can be expressed as follows:

$$\begin{aligned} SP4.1: \max_{\boldsymbol{\Psi}(n)} \quad & \left| h_m^d(n) + \left(\boldsymbol{h}_m^r(n)\right)^H \boldsymbol{\Phi}_m(n) \boldsymbol{h}^u(n) \right|^2 \\ \text{s.t.} \quad & 0 \le \phi_{m_x, m_y}^m(n) < 2\pi. \end{aligned} \tag{42}$$

Although problem $SP4.1$ is non-convex, its special structural properties enable us to derive a closed-form solution. Specifically, by leveraging the triangle inequality, we obtain the following result:

$$\begin{aligned}&\left|h_m^d(n)+\left(\boldsymbol{h}_m^r(n)\right)^H\boldsymbol{\Phi}_m(n)\boldsymbol{h}^u(n)\right|^2\\ \leq&\left|h_m^d(n)\right|^2+\left|\left(\boldsymbol{h}_m^r(n)\right)^H\boldsymbol{\Phi}_m(n)\boldsymbol{h}^u(n)\right|^2.\end{aligned}\tag{43}$$

Inequality (43) becomes equality if and only if $\arg\big(\left(\boldsymbol{h}_m^r(n)\right)^H\boldsymbol{\Phi}_m(n)\boldsymbol{h}^u(n)\big) = \arg\big(h_m^d(n)\big)$. Subsequently, let $\left(\boldsymbol{h}_m^r(n)\right)^H\boldsymbol{\Phi}_m(n)\boldsymbol{h}^u(n) = \boldsymbol{w}(n)\boldsymbol{I}_m(n)$, where $\boldsymbol{w}(n) = [w_1(n),...,w_{M_x\times M_y}(n)]^{\mathrm{H}} = \big[\exp\big(j\phi_{1,1}^m(n)\big),...,\exp\big(j\phi_{M_x,M_y}^m(n)\big)\big]^{\mathrm{H}}$ and $\boldsymbol{I}_m(n) = \mathrm{diag}\big(\boldsymbol{h}_m^r(n)^H\big)\boldsymbol{h}^u(n)$. Therefore, based (43), problem $SP4.1$ is equivalent to

$$\begin{aligned}SP4.2:\ \max_{\boldsymbol{w}(n)}\quad&\left|\boldsymbol{w}(n)\boldsymbol{I}_m(n)\right|^2\\ \text{s.t.}\quad&|w_{m_x\times m_y}(n)|=1,\\ &\arg\big(\boldsymbol{w}(n)\boldsymbol{I}_m(n)\big)=\arg\big(h_m^d(n)\big).\end{aligned}\tag{44}$$

It is tractable to find that the optimal solution to $SP4.1$ is $\boldsymbol{w}(n)^* = \exp\big(j\big[\arg\big(h_m^d(n)\big) - \arg\big(\boldsymbol{I}_m(n)\big)\big]\big)$. Thus, the optimal phase shift of m-th UD in the m_x-th row and m_y-th array element is given by

$$\begin{aligned}&\phi_{m_x,m_y}^m(n)^*\\ =&\arg\big(h_m^d(n)\big)-\arg\big(I_{m_x\times m_y}^m(n)\big)\\ =&\arg\big(h_m^d(n)\big)-\arg\big(\big[\psi_{m_x,y_x}^m(n)\big]^{\mathrm{H}}\psi_{m_x,y_x}^u(n)\big)\\ =&\arg\big(h_m^d(n)\big)+\arg\big(\psi_{m_x,y_x}^m(n)\big)-\arg\big(\psi_{m_x,y_x}^u(n)\big),\end{aligned}\tag{45, 46}$$

where $I_{m_x\times m_y}^m(n)$, $\psi_{m_x,y_x}^m(n)$, and $\psi_{m_x,y_x}^u(n)$ are the m_x-th row and m_y-th array element in $\boldsymbol{I}_m(n)$, $\boldsymbol{h}_m^r(n)$ and $\boldsymbol{h}^u(n)$. At this point, we have obtained the optimal RIS phase shift. Furthermore, once the optimal phase angle $\phi_{m_x,m_y}^m(n)^*$ is determined, the channel gain $h_m(n)$ attains a constant complex value. Consequently, problem $SP4$ simplifies into a convex optimization problem concerning solely $P_m(n)$. Analogous to the approach employed for solving sub-problems $SP1$ and $SP2$, a closed-form solution for the optimal transmit power can be formulated.

D. UAV Trajectory Optimization

The trajectory of the UAV affects both flying energy consumption and channel gain. By isolating these two factors from the problem $P2$, the sub-problem of the UAV trajectory optimization can be obtained as follows

$$\begin{aligned}SP5:\min_{\boldsymbol{S}_U(n)}\ &V_L\varepsilon e_f(n)+\sum_{m\in\boldsymbol{M}}\left\{\frac{3}{2}D_m^o(n)^2+C_m^2(n)D_m^o(n)\right\}\\ \text{s.t.}\ \ &C7,C8.\end{aligned}\tag{47}$$

where $e_f(n)$ and $D_m^o(n)$ are influenced by $\boldsymbol{S}_u(n)$. Mathematically, solving $SP5$ presents significant challenges due to the constraint $C8$ and its non-convex nature. Similar to reference [27], to efficiently tackle this knotty problem, we firstly use the penalty function method to eliminate constraint $C8$. Although this method loses some accuracy, it significantly reduces the computational complexity of the problem, which is in line with the needs of practical engineering. Without loss of generality, a penalty factor μ is introduced, which increases with the growth of the slot. Thereafter, the sub-problem $SP5$ can be transformed into

$$\begin{aligned}SP5.1:\min_{\boldsymbol{S}_U(n)}\ &V_L\varepsilon e_f(n)+\mu\|\boldsymbol{S}_U(n)-\boldsymbol{S}_F\|_2^2\\ &+\sum_{m\in\boldsymbol{M}}\left\{\frac{3}{2}D_m^o(n)^2+C_m^2(n)D_m^o(n)\right\}\\ \text{s.t.}\ \ &\frac{\|\boldsymbol{S}_U(n)-\boldsymbol{S}_U(n-1)\|_2}{\delta_t}\leq v_{max}.\end{aligned}\tag{48}$$

The above problem eliminates the constraint of long-term trajectory, but it is worth noting that when $n=1$, $\boldsymbol{S}_U(n) = \boldsymbol{S}_I$. To further address the non-convex sub-problem $SP5.1$, we devise a low-complexity algorithm based on the SCA technique. Compared with existing algorithms, this algorithm thoroughly approximates $SP5.1$ as a simple convex problem to obtain closed-form optimal solutions for each iteration, and facilitates the scheduling of the UAV trajectory through successive updates. Specifically, we denote $[\cdot]^k$ as the value at the k-th iteration's expansion point. Utilizing the first-order Taylor expansion, we can enable an approximate transformation of $D_m^o(n)$ as follows:

$$\begin{aligned}D_m^o(n)\approx&D_m^o(n)^k+\left.\frac{\partial D_m^o(n)}{\partial x_U(n)}\right|_{x_U(n)^k}[x_U(n)-x_U(n)^k]\\ &+\left.\frac{\partial D_m^o(n)}{\partial y_U(n)}\right|_{y_U(n)^k}[y_U(n)-y_U(n)^k].\end{aligned}\tag{49}$$

It is worth noting that the iterative process of SCA method can not only effectively handle non-convex functions, but also correct errors introduced by truncating high-order Taylor expansion terms, thereby ensuring the accuracy of the algorithm, especially in the case of high-speed UAV flight. Similarly, using $v(n)^k$ as the expansion point, the non-convex portion of flying energy consumption is also addressed, therefore, the energy consumption of UAV flying can be approximated as

$$\begin{aligned}e_f(n)\approx&\delta_tP_o\left(1+\frac{3v(n)^2}{\Omega^2{r_f}^2}\right)+\frac{\delta_td_0\rho_fs_fA_r}{4}\left\{3v(n)^kv(n)^2\right.\\ &\left.-[v(n)^k]^3\right\}+\frac{\delta_tP_iv_0}{[v(n)^k]^2}\left\{2-\frac{v(n)^2}{[v(n)^k]^2}\right\}\\ =&{\delta_t}^2\left\{\frac{3P_o}{\delta_t\Omega^2{r_f}^2}+\frac{3d_0\rho_fs_fA_rv(n)^k}{4\delta_t}-\frac{P_iv_0}{\delta_t[v(n)^k]^4}\right\}v(n)^2\\ &+\delta_tP_o-\frac{\delta_td_0\rho_fs_fA_r}{4}[v(n)^k]^3+\frac{2\delta_tP_iv_0}{[v(n)^k]^2}\\ \triangleq&{\delta_t}^2C^3(n)v(n)^2+C^4(n).\end{aligned}\tag{50}$$

where $C^3(n)$ and $C^4(n)$ are constants related to the expansion point and system environment parameters. Following algebraic manipulations, the objective function for sub-problem $P5.1$ is reformulated as $F\big(\boldsymbol{S}_u(n)\big)$, detailed in (51).

$$
\begin{aligned}
&F\big(\boldsymbol{S}_u(n)\big)\\
&=\underbrace{\left\{V_L\varepsilon C^3(n)+\mu+\frac{3}{2}\sum_{m\in\boldsymbol{M}}\left[\frac{\partial D_m^o(n)}{\partial x_U(n)}\Big|_{x_U(n)^k}\right]^2\right\}}_{C_A(n)^k}x_U(n)^2\\
&+\underbrace{\left\{V_L\varepsilon C^3(n)+\mu+\frac{3}{2}\sum_{m\in\boldsymbol{M}}\left[\frac{\partial D_m^o(n)}{\partial y_U(n)}\Big|_{y_U(n)^k}\right]^2\right\}}_{C_B(n)^k}y_U(n)^2\\
&+\underbrace{3\sum_{m\in\boldsymbol{M}}\left\{\frac{\partial D_m^o(n)}{\partial x_U(n)}\Big|_{x_U(n)^k}\frac{\partial D_m^o(n)}{\partial y_U(n)}\Big|_{y_U(n)^k}\right\}}_{C_C(n)^k}x_U(n)y_U(n)\\
&-2\underbrace{\left\{V_L\varepsilon C^3(n)x_U(n-1)+\mu x_F-\sum_{m\in\boldsymbol{M}}\frac{3C_m^5(n)+C_m^2(n)}{2}\frac{\partial D_m^o(n)}{\partial x_U(n)}\Big|_{x_U(n)^k}\right\}}_{C_D(n)^k}x_U(n)\\
&-2\underbrace{\left\{V_L\varepsilon C^3(n)y_U(n-1)+\mu y_F-\sum_{m\in\boldsymbol{M}}\frac{3C_m^5(n)+C_m^2(n)}{2}\frac{\partial D_m^o(n)}{\partial y_U(n)}\Big|_{y_U(n)^k}\right\}}_{C_E(n)^k}y_U(n)\\
&+\underbrace{V_L\varepsilon\Big\{C^3(n)\big[x_U(n-1)^2+y_U(n-1)^2\big]+C^4(n)\Big\}+\mu\big[{x_F}^2+{y_F}^2\big]+\sum_{m\in\boldsymbol{M}}\Big\{C_m^5(n)^2+C_m^2(n)C_m^5(n)\Big\}.}_{C_F(n)^k}
\end{aligned}
\tag{51}
$$

Based on formula (51), problem $SP5.1$ can be further rewritten as

$$
\begin{aligned}
SP5.2:\min_{\boldsymbol{S}_U(n)}\quad & C_A(n)^k x_U(n)^2+C_B(n)^k y_U(n)^2\\
&+C_C(n)^k x_U(n)y_U(n)+C_D(n)^k x_U(n)\\
&+C_E(n)^k y_U(n)+C_F(n)^k\\
\text{s.t.}\quad & \|\boldsymbol{S}_U(n)-\boldsymbol{S}_U(n-1)\|_2\le\delta_t v_{max}.
\end{aligned}
\tag{52}
$$

Obviously, sub-problem $SP5.2$ exemplifies a typical convex optimization challenge. Similar to sub-problems $SP1$ and $SP2$, by computing the partial derivatives of the objective function with respect to $x_U(n)$ and $y_U(n)$, we can derive

$$
\begin{cases}
\dfrac{\partial F\big(\boldsymbol{S}_U(n)\big)}{\partial x_U(n)}=2C_A(n)^k x_U(n)+C_C(n)^k y_U(n)+C_D(n)^k, & \text{(53a)}\\
\dfrac{\partial F\big(\boldsymbol{S}_U(n)\big)}{\partial y_U(n)}=2C_B(n)^k y_U(n)+C_C(n)^k x_U(n)+C_E(n)^k. & \text{(53b)}
\end{cases}
$$

Setting equations (52a) and (52b) to zero and solving them simultaneously allows us to determine the extremum values for the variables involved, which yields

$$
\begin{cases}
{x_U}'(n)=\dfrac{C_C(n)^k C_E(n)^k-2C_B(n)^k C_D(n)^k}{4C_A(n)^k C_B(n)^k-[C_C(n)^k]^2}, & \text{(54a)}\\
{y_U}'(n)=\dfrac{C_C(n)^k C_D(n)^k-2C_A(n)^k C_E(n)^k}{4C_A(n)^k C_B(n)^k-[C_C(n)^k]^2}. & \text{(54b)}
\end{cases}
$$

Define the position of the UAV at the extremum point as $\boldsymbol{S}_U{}'(n)=\{x_U{}'(n),y_U{}'(n),H_U\}$. Considering the constraint of maximum flying speed, we encounter two distinct scenarios:

Case 1: If $\|\boldsymbol{S}_U{}'(n)-\boldsymbol{S}_U(n-1)\|\le\delta_t v_{max}$, then optimal trajectory at n-th slot is just the point $\boldsymbol{S}_U{}^*(n)=\boldsymbol{S}_U{}'(n)$.

Case 2: If $\|\boldsymbol{S}_U{}'(n)-\boldsymbol{S}_U(n-1)\|>\delta_t v_{max}$, given the maximum velocity constraint, the optimal solution point must align in the same direction as the maximum velocity. By applying proportional scaling, we can adjust the trajectory to meet these constraints, thereby deriving a revised optimal trajectory:

$$
\begin{cases}
{x_U}^*(n)=\dfrac{\delta_t v_{max}[x_U{}'(n)-x_U(n-1)]}{\|\boldsymbol{S}'_U(n)-\boldsymbol{S}_U(n-1)\|_2}+x_U(n-1), & \text{(55a)}\\
{y_U}^*(n)=\dfrac{\delta_t v_{max}[y_U{}'(n)-y_U(n-1)]}{\|\boldsymbol{S}'_U(n)-\boldsymbol{S}_U(n-1)\|_2}+y_U(n-1). & \text{(55b)}
\end{cases}
$$

Thereafter, by using the solved optimal trajectory $\boldsymbol{S}_u{}^*(n)$ as the expansion point for the $(k+1)$-th iteration, we can approach an asymptotically optimal solution, which is achieved when the variation in the final trajectory between iterations falls below the threshold σ_U.

VI. Algorithm Analysis

In this section, we evaluate the performance of the proposed online algorithm, focusing on metrics such as the upper bounds of queue backlog and energy consumption, as well as the complexity of the algorithm.

Firstly, we establish the tradeoff between system stability and energy consumption in the Theorem 1.

Theorem 1. *Assuming that the stability and energy consumption tradeoff problem is feasible, then*

- *The time-average sum of all queue backlogs is bounded by*

$$
\lim_{\mathrm{N}\to\infty}\frac{1}{\mathrm{N}}\sum_{n=0}^{\mathrm{N}-1}\mathbb{E}\{\boldsymbol{\mathcal{Q}}(n)\}\le\frac{[F_{max}^u\delta_t]^2}{\epsilon\varphi^2}+V_L\frac{E^{opt}}{\epsilon},
\tag{56}
$$

where E^{opt} is the optimal long-term energy consumption of the system.

- *The average energy consumption of the network, as determined by the proposed algorithm, is upper bounded by*

$$
\begin{aligned}
&\lim_{\mathrm{N}\to\infty}\frac{1}{\mathrm{N}}\sum_{n=0}^{N-1}\mathbb{E}\left\{\varepsilon e_u(n)+e_f(n)+\sum_{m\in\boldsymbol{M}}\Big\{e_m(n)+e_m^p(n)\Big\}\right\}\\
&\le\frac{[F_{max}^u\delta_t]^2}{V_L\varphi^2}+E^{opt}.
\end{aligned}
\tag{57}
$$

Proof. Please refer to Appendix A. □

Theorem 1 illustrates that the queue backlog expands in proportion to V_L, and the average energy consumption declines as the V_L increases. By assigning a sufficiently large value to

the V_L, we can approximate the optimal energy consumption E^{opt}. This relationship highlights a tradeoff between average energy consumption and queue backlog.

In the following, we will prove the convergence of the proposed algorithm. we denote the objective function of problem $P2$ as $F\{\boldsymbol{F}(n)^l,\ f_u(n)^l,\ \boldsymbol{\tau}(n)^l,\ \boldsymbol{\Psi}(n)^l,\ \boldsymbol{P}(n)^l,\ \boldsymbol{S}_U(n)^l\}$, where $[\cdot]^l$ represents separately the value obtained after the l-th alternating iteration. Consequently, the following inequality relationship can be obtained

$$\begin{aligned}
&F\{\boldsymbol{F}(n)^l, f_u(n)^l,\ \boldsymbol{\tau}(n)^l, \boldsymbol{\Psi}(n)^l, \boldsymbol{P}(n)^l, \boldsymbol{S}_U(n)^l\}\\
\geq&F\{\boldsymbol{F}(n)^{l+1}, f_u(n)^{l+1}, \boldsymbol{\tau}(n)^l, \boldsymbol{\Psi}(n)^l, \boldsymbol{P}(n)^l, \boldsymbol{S}_U(n)^l\}\\
\geq&F\{\boldsymbol{F}(n)^{l+1}, f_u(n)^{l+1}, \boldsymbol{\tau}(n)^{l+1}, \boldsymbol{\Psi}(n)^l, \boldsymbol{P}(n)^l, \boldsymbol{S}_U(n)^l\}\\
\geq&F\{\boldsymbol{F}(n)^{l+1}, f_u(n)^{l+1}, \boldsymbol{\tau}(n)^{l+1}, \boldsymbol{\Psi}(n)^{l+1}, \boldsymbol{P}(n)^{l+1}, \boldsymbol{S}_U(n)^l\}\\
\geq&F\{\boldsymbol{F}(n)^{l+1}, f_u(n)^{l+1}, \boldsymbol{\tau}(n)^{l+1}, \boldsymbol{\Psi}(n)^{l+1}, \boldsymbol{P}(n)^{l+1},\\
&\boldsymbol{S}_U(n)^{l+1}\}. \qquad (58)
\end{aligned}$$

Thus, the objective function of problem $P2$ is monotonically non-increasing after each iteration. Moreover, since both the system energy consumption and Lyapunov drift have the lower-bounded, the objective function F must converge after several iterations and the gap of convergence each time will not exceed σ_A.

Finally, we provide a brief analysis of the complexity of the proposed algorithm. Firstly, the complexity of the algorithm mainly consists of two aspects: one is the process of solving two sub-problems; the other is the iteration process of alternating optimization. For the first part, since closed-form solutions for computational resources, reflection angles, and transmit power can be derived directly, the complexity of our algorithm primarily arises from slots allocation and trajectory optimization. Considering that the algorithm is linear convergence, the complexity of the slots allocation and trajectory optimization are $\mathcal{O}(\log_2(1/\sigma_\tau))$ and $\mathcal{O}(\log_2(1/\sigma_U))$. Similarly, the complexity of the latter is $\mathcal{O}(\log_2(1/\sigma_A))$. Furthermore, due to the nested nature of the above two processes, the complexity of proposed algorithm for each time slot is $\mathcal{O}(\log_2(1/\sigma_\tau\sigma_U)\log_2(1/\sigma_A))$, and the total complexity of the algorithm is $\mathcal{O}(\mathrm{N}\log_2(1/\sigma_\tau\sigma_U)\log_2(1/\sigma_A))$.

TABLE I
SIMULATION PARAMETERS

Parameters	**Value**
Channel bandwidth	W=0.1MHz
Maximum transmit power	P_{max}=0.5W
Noise power density	N_0=-130dBW/Hz
Communication carrier wavelength	λ_r = 0.125m
The excessive path loss of LoS	η_{LoS}=0.1
The excessive path loss of NLoS	η_{NLoS}= 21
The constant values of environment	A=9.61, B= 0.16
Process density	φ=1000cycles/bit
The average tasks arrival rate	λ=1.5Mbit/s
Effective switched capability	κ=10^{-27}
Blade profile power	P_o=79.86W
Induced power	P_i=88.63W
Blade angular velocity	Ω=300rad/s
Rotor radius	r_f=0.4m
Rotor disc area	A_r=0.503m^2

VII. Simulation Results

Our evaluation of the proposed algorithm focuses on the average queue backlog and total energy consumption, utilizing detailed numerical simulations. Without loss of generality, we simulate a scenario involving a UAV, a RIS, and fifteen UDs, they are distributed in $500 \times 500\mathrm{m}^2$. The UAV starts at $\boldsymbol{S}_I = \{0, 0, 200\}$ and moves to $\boldsymbol{S}_F = \{500, 0, 200\}$, maintaining a maximum speed of $v_{max} = 15$ m/s. Moreover, the coordinate of the RIS is $\boldsymbol{S}_R = \{250, 500, 50\}$. Considering the system's runtime is always limited in practical systems, the operation period of the UAV spans N = 300 slots, each lasting $\delta_t = 1$s. Parameter selection is guided by established industry standards and data sheets, referenced in [33], with critical simulation parameters outlined in Table I. Furthermore, in order to simulate real-world conditions as realistically as possible, we have incorporated dynamic and unexpected factors (such as the random fluctuation of channel) into the simulation, which means that our simulation design has high fidelity and partly represents actual engineering scenarios.

To validate the effectiveness of the proposed scheme, we conducted comparative analyses against three baseline algorithms. "Full local algorithm" represents that UDs perform all local computing tasks without relying on the UAV. "Random algorithm" refers to UD randomly selecting the current strategy. "The algorithm in [33]" embodies an enhanced metaheuristic approach. Moreover, to mitigate the impact of random variability on the simulation results, this work conducted 50 independent simulations. The results from these simulations were then statisticaly averaged to ensure a more reliable and robust analysis.

Fig. 3 illustrates the relationship between the average queue backlog of UAV and UDs and average energy consumption of system under different Lyapunov control factors. Intuitively, as the control factor gradually increases, the average queue backlog increases while energy consumption decreases, which confirms that the control factor can indeed achieve a tradeoff between system efficiency and energy consumption. Furthermore, the queue backlog exhibits a linear upward trend, while the decreased rate of energy consumption gradually decelerates with the increase of V_L, which validates the conclusion drawn in Theorem 1. It is worth noting that although the queue backlogs for UAV and UDs are increasing synchronizedly, the backlog of UAV remains consistently smaller than that of UDs, meanwhile, the growth rate of the UAV backlog is also lower than that of UDs, thanks to the relatively abundant computing resources available to UAVs.

Fig. 4 shows the changes in energy consumption under different time slot lengths as the number of UDs increases. Specifically, with an increase in the number of UDs, the competition for system resources intensifies, necessitating higher energy expenditure by each UD to ensure the stable operation of the system. Consequently, as illustrated in Fig. 4, the overall energy consumption escalates as the number of UD increases. Furthermore, the duration of the time slots significantly influences energy consumption. Notably, when the slot length decreases from $\delta_t = 1.5$ s to $\delta_t = 0.5$ s, both the energy consumption and its rate of increase are decreasing. This efficiency gain arises because shorter slot

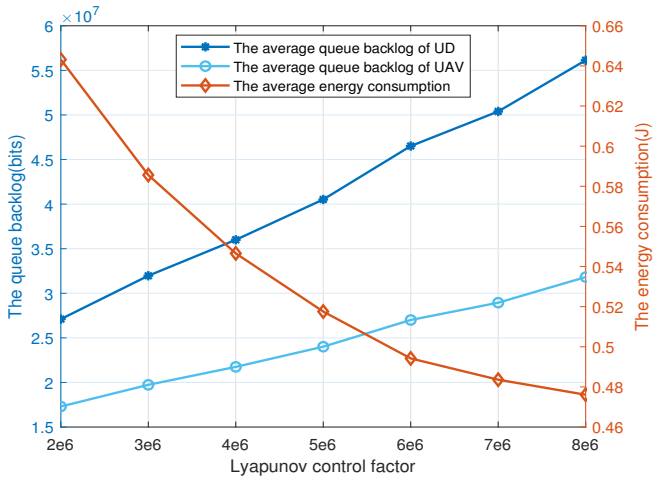

Fig. 3. The queue backlog and energy consumption under different V_L.

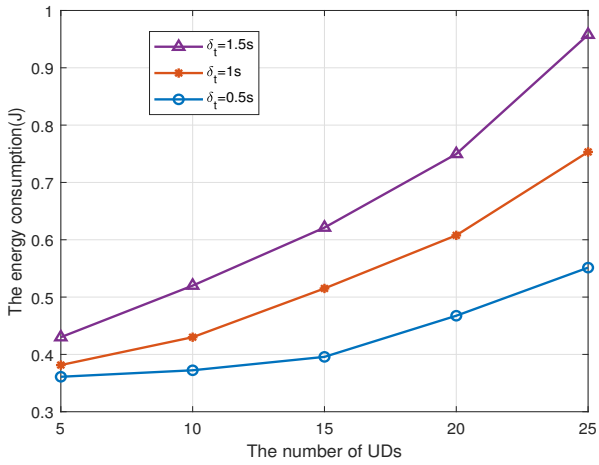

Fig. 4. Energy consumption under different M and δ_t.

lengths allow for quicker responses to UDs' demands within the system. Additionally, the flexibility in resource allocation and trajectory optimization is enhanced, facilitating optimal utilization of system resources.

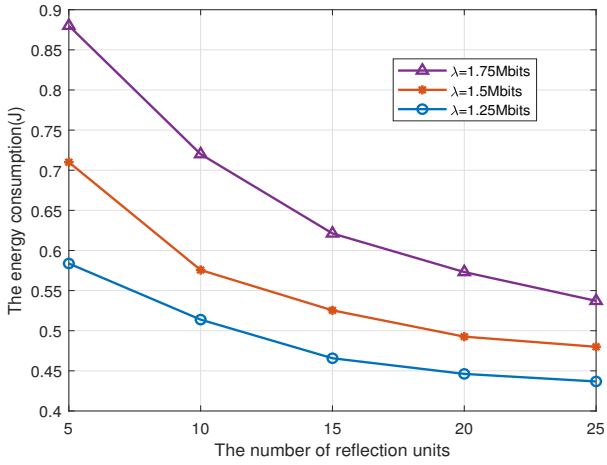

Fig. 5. Energy consumption under different M_R and λ.

Fig. 5 displays the changes in energy consumption under different average task arrivals as the number of reflection units increases. Fig. 5 demonstrates that as the number of reflection units increases, there is a notable reduction in energy consumption across various average task arrivals. There are two reasons for this reduction. Firstly, the addition of more reflection units enhances the virtual link gain, which directly reduces the energy required for transmission. Secondly, these better channel conditions encourage UDs to offload more tasks to the UAV. This shift enables more effective use of computational resources at both the UDs and UAV, leading to further optimizations in energy consumption. Moreover, overall energy consumption remains relatively high when the average task arrival is elevated, the trend of decreasing energy consumption becomes most pronounced as the number of reflection units grows. This indicates that the benefits of improved channel conditions are amplified under higher task arrival, effectively mitigating energy demands.

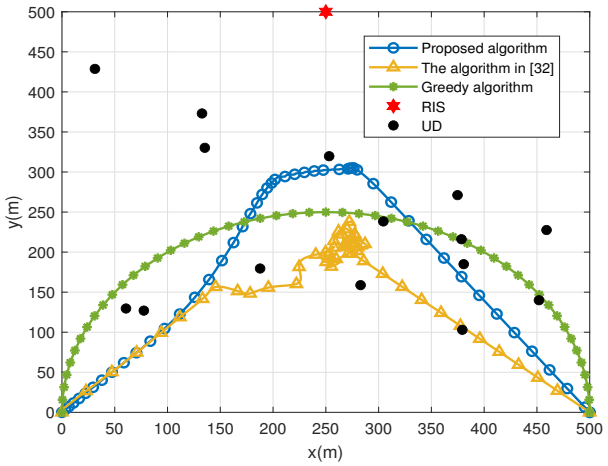

Fig. 6. The flying trajectories under different schemes

Fig. 6 shows the flying trajectories of UAV under different schemes, including the proposed algorithm, the algorithm in [33], and the random algorithm. The trajectory of the proposed algorithm initially directs the UAV towards the center of the service area, and then circles in the center, before ultimately returning to the endpoint, which presents a smoother arched path. In contrast, the trajectory generated by the algorithm in [33] adopts a more conservative approach, where the UAV hovers at the center of the UD cluster. It is worth noting that the trajectories of the above algorithms hover around the RIS position, highlighting the crucial role of RIS in enhancing communication. Furthermore, for the random algorithm, we designed a semi-circular flight path from the starting point to the endpoint. Meanwhile, the full local algorithm does not involve the flying trajectory since it operates without UAV assistance, focusing solely on local computing resources.

Fig. 7 exhibits the variation of task backlog with slots under different schemes. Firstly, the queue backlog for both the full local algorithm and the random algorithm tends to become unstable. This instability arises from relying solely on the UDs or from mismanaging resources at both ends, which can lead to an increasing task backlog. Secondly, both the proposed algorithm and the algorithm in [33] show that the task backlogs tend to stabilize as the number of time slots increases. However, graphical analysis reveals that compared with baseline algorithms, the task backlog values for the

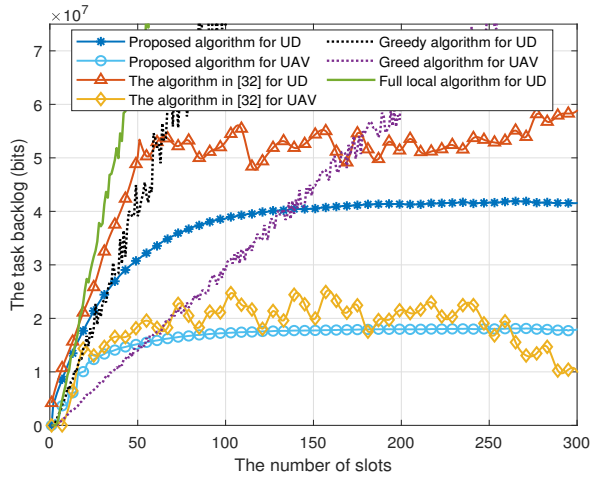

Fig. 7. The variation of task backlog with slots under different schemes.

proposed algorithm are consistently lower and more stable, which is attributed to the smaller gap between the upper bound of the Lyapunov drift function and the original function. In the optimization process, a smaller gap can ensure that the optimization effect is better transmitted to the original function, thereby minimizing the variation of the drift function and maintaining a lower and more stable system backlog.

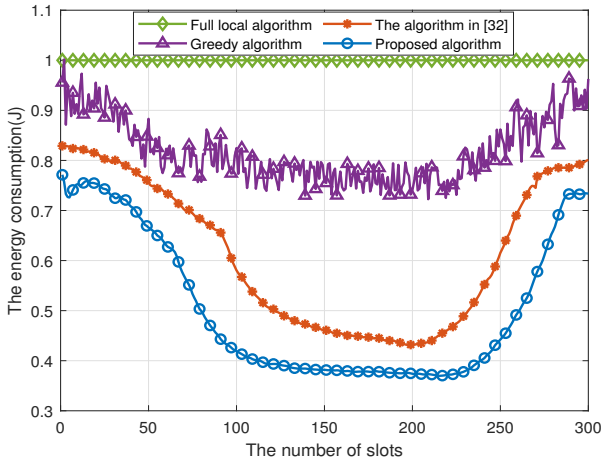

Fig. 8. The variation of energy consumption with slots under different schemes.

Fig. 8 shows the variation of energy consumption with slots under different schemes. Due to the inability of local computing resources to fully process generated tasks, UDs consistently operate at maximum computing frequencies, leading to the highest energy consumption. Moreover, the random algorithm, characterized by its stochastic strategy selection, exhibits significant fluctuations in energy consumption. However, both the proposed algorithm and the algorithm in [33] strategically optimize the allocation and utilization of system resources, resulting in markedly lower energy consumption compared to the aforementioned algorithms. Under these optimized algorithms, it is observed that at the onset of task processing, total energy consumption progressively declines with an increase in time slots. This reduction is primarily because UAV, aiming to handle more tasks efficiently, fly toward the UD center to achieve better channel gains, thus reducing energy consumption. Once the UAV reaches a central area with optimal channel gain, it hovers there for a duration to process tasks, maintaining low energy consumption during this period. Finally, as the UAV departs from this area, the channel gain decreases and energy consumption rises once more. Additionally, the proposed algorithm demonstrates superior energy efficiency due to its effective optimization capabilities.

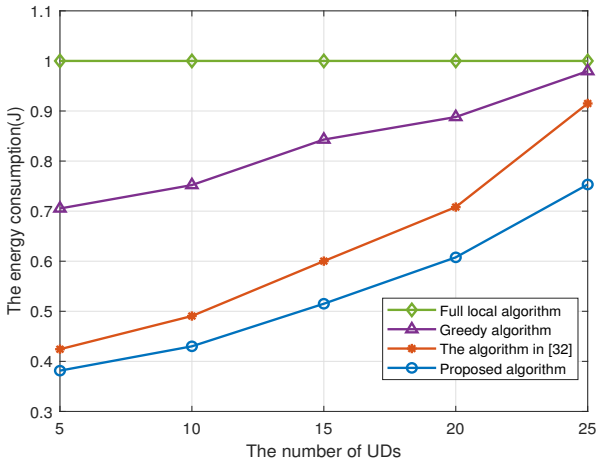

Fig. 9. Energy consumption with the number of UDs under different schemes.

In Fig. 9, we have drawn the change curves of the energy consumption for our proposed algorithm and three benchmark methods with the number of UDs. From Fig. 9, it can be seen that full local algorithms maintain the highest energy consumption due to the limited computing resources. Additionally, The energy consumption of the other three algorithms increases continuously with the increase in the number of UDs, among which the proposed algorithm exhibits the lowest energy consumption and the most gradual growth rate, attributable to two key strategies. Firstly, the adoption of the TDMA system enhances spectral efficiency. Utilizing this system allows for coherent signal accumulation through the strategic adjustment of the RIS reflection angles, which substantially boosts channel gain. Secondly, although the proposed algorithm employs alternating optimization to approach the optimal solution, the sub-problem solutions leverage convex optimization principles. This approach facilitates the development of high-precision algorithms that are either of lower complexity or yield direct closed-form optimal solutions. Consequently, the proposed algorithm achieves near-optimal solutions with greater accuracy and reduced complexity.

In Fig. 10, we compare the number of iterations between the proposed algorithm and the algorithm referenced in [33] as the number of UDs varies. From Fig. 10, it can be intuitively seen that as the number of UDs increases, the number of iterations of the proposed algorithm shows a linear growth trend, while the algorithm in [33] shows an exponential growth trend. This is because an increase in the number of UDs leads to a rapid expansion of the policy space, and the algorithm in [33] is an improved metaheuristic algorithm, where an increase in the policy space greatly increases the difficulty of searching for the optimal solution. It is worth noting that the growth rate of the proposed algorithm is basically consistent with the theoretical algorithm complexity obtained in Theorem 1. In addition, due

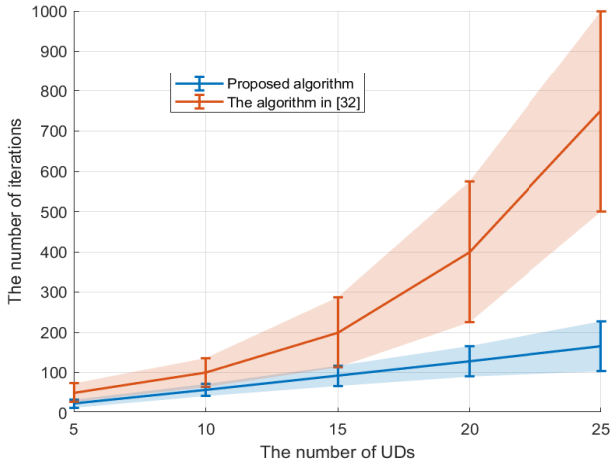

Fig. 10. The number of iterations with the number of UDs under different schemes.

to the robustness and stability of the proposed algorithm, the increase in the number of UDs has a relatively small impact on the variance of the iteration times of the proposed algorithm.

VIII. Conclusion

This paper discusses the long-term performance of the RIS-assisted UAV-enabled MEC network model, which is an innovative work. The model aims to optimize the allocation of computing resources, time slot rate, transmitpower, RIS phase angles, and flight trajectories to reduce long-term energy consumption while ensuring system stability. We use the Lyapunov method to transform complex long-term stochastic optimization problem into more manageable deterministic sub-problems. Subsequently, the approximately optimal allocation of computing resources and time slot rate are obtained by utilizing convex optimization theory. Moreover, the optimal RIS phase and transmit power are obtained by adjusting the phase to achieve coherent signal accumulation. Finally, the trajectory planning algorithm is designed using techniques such as the SCA and internal penalty function. The simulation results show that the proposed algorithm can achieve lower long-term energy consumption while ensuring system stability. In future work, we will promote multi UAV systems, multi antenna UAV, and active RIS to provide UD with more satisfactory services.

Appendix A
Proof of Theorem 1

Assuming that problem $P2$ is feasible, and given a task with an arrival rate λ, for all time slots and any $\sigma > 0$, it can be demonstrated that there exists an independent and stable resource allocation and trajectory optimization algorithm. Given a positive constant ϵ, the system state under this algorithm satisfies the following inequality:

$$\mathbb{E}\{\sum_{m\in\boldsymbol{M}} A_m(n)\big|\boldsymbol{\mathcal{Q}}(n)\} \le \mathbb{E}\{\sum_{m\in\boldsymbol{M}}[D_m(n)+D_m^o(n)]\big|\boldsymbol{\mathcal{Q}}(n)\} - \epsilon, \tag{59}$$

$$\mathbb{E}\{\sum\nolimits_{m\in\boldsymbol{M}} D_m^o(n)\big|\boldsymbol{\mathcal{Q}}(n)\} \le \mathbb{E}\{D_u(n)\big|\boldsymbol{\mathcal{Q}}(n)\} - \epsilon, \tag{60}$$

$$\mathbb{E}\{\sum\nolimits_{m\in\boldsymbol{M}} e_m(n)\big|\boldsymbol{\mathcal{Q}}(n)\} \leqslant \sum\nolimits_{m\in\boldsymbol{M}} e_m^{opt} + \sigma, \tag{61}$$

$$\mathbb{E}\{\sum\nolimits_{m\in\boldsymbol{M}} e_m^p(n)\big|\boldsymbol{\mathcal{Q}}(n)\} \leqslant \sum\nolimits_{m\in\boldsymbol{M}} e_m^{p,opt} + \sigma, \tag{62}$$

$$\mathbb{E}\{\varepsilon e_f(n)|\boldsymbol{\mathcal{Q}}(n)\} \leqslant \varepsilon e_f^{opt} + \sigma, \tag{63}$$

$$\mathbb{E}\{e_u(n)|\boldsymbol{\mathcal{Q}}(n)\} \leqslant e_u^{opt} + \sigma. \tag{64}$$

Due to spatial constraints, the proof of the aforementioned inequality will not be included here. However, similar proofs are available in reference [43]. Subsequently, we reorganize inequality (29), then set $\sigma \to 0$, and incorporate inequalities (59) through (64) into the restructured equation, which can yield as

$$\begin{aligned}\mathcal{D}(n) \le& \mathbb{E}\Big\{D_u(n)^2+\Big[\sum\nolimits_{m\in\boldsymbol{M}} D_m^o(n)\Big]^2 - D_u(n)\sum\nolimits_{m\in\boldsymbol{M}} D_m^o(n) \\ &+ \sum\nolimits_{m\in\boldsymbol{M}}\Big\{\frac{A_m(n)^2}{2} - \frac{[D_m(n)+D_m^o(n)]^2}{2}\Big\}\Big|\boldsymbol{\mathcal{Q}}(n)\Big\} \\ &- \epsilon\cdot\mathbb{E}\Big\{L(n)+\sum\nolimits_{m\in\boldsymbol{M}} Q_m(n)\Big|\boldsymbol{\mathcal{Q}}(n)\Big\} \\ &+ V_L\Big[e_u^{opt}(n)+\varepsilon e_f^{opt}+\sum\nolimits_{m\in\boldsymbol{M}}\{e_m^{opt}+e_m^{p,opt}\}\Big] \\ \le& \Big[\frac{F_{max}^u\delta_t}{\varphi}\Big]^2 - \epsilon\cdot\mathbb{E}\Big\{L(n)+\sum\nolimits_{m\in\boldsymbol{M}} Q_m(n)\Big|\boldsymbol{\mathcal{Q}}(n)\Big\} \\ &+ V_L\Big[e_u^{opt}(n)+\varepsilon e_f^{opt}+\sum\nolimits_{m\in\boldsymbol{M}}\{e_m^{opt}+e_m^{p,opt}\}\Big].\end{aligned} \tag{65}$$

By summing the given inequality across all time slots, excluding $n = \mathrm{N}$, while applying the queue scaling sum property, we derive:

$$\begin{aligned}&\mathbb{E}\{V(\mathrm{N})-V(0)\} \\ &+ V_L\sum_{n\in\boldsymbol{N}\setminus\mathrm{N}}\mathbb{E}\Big\{\varepsilon e_u(n)+e_f(n)+\sum_{m\in\boldsymbol{M}}\Big\{e_m(n)+e_m^p(n)\Big\}\Big\} \\ \leqslant& \mathrm{N}\Big[\frac{F_{max}^u\delta_t}{\varphi}\Big]^2 - \epsilon\sum\nolimits_{n\in\boldsymbol{N}\setminus\mathrm{N}}\mathbb{E}\{\boldsymbol{\mathcal{Q}}(n)\} \\ &+ \mathrm{N}V_L\Big[e_u^{opt}(n)+\varepsilon e_f^{opt}+\sum_{m\in\boldsymbol{M}}\{e_m^{opt}+e_m^{p,opt}\}\Big].\end{aligned} \tag{66}$$

Considering that the system queue starts from an empty state, where $\mathbb{E}\{V(0)\} = 0$, it eventually reaches a steady state as N approaches infinity. In this context, $\mathbb{E}\{V(\mathrm{N})\}$ remains bounded by constants. By allowing $\mathrm{N}\to\infty$, dividing both sides of the inequality by $\mathrm{N}\epsilon$, and neglecting certain non-negative terms, the following result is obtained:

$$\begin{aligned}&\lim_{\mathrm{N}\to\infty}\frac{1}{\mathrm{N}}\sum_{n=0}^{\mathrm{N}-1}\mathbb{E}\{\boldsymbol{\mathcal{Q}}(n)\} \\ \le& \frac{[F_{max}^u\delta_t]^2}{\epsilon\varphi^2} + \frac{V_L\Big[e_u^{opt}(n)+\varepsilon e_f^{opt}+\sum_{m\in\boldsymbol{M}}\{e_m^{opt}+e_m^{p,opt}\}\Big]}{\epsilon} \\ \triangleq& \frac{[F_{max}^u\delta_t]^2}{\epsilon\varphi^2} + V_L\frac{E^{opt}}{\epsilon},\end{aligned} \tag{67}$$

where $E^{opt} = e_u^{opt}(n) + \varepsilon e_f^{opt} + \sum_{m\in\boldsymbol{M}} \left\{e_m^{opt} + e_m^{p,opt}\right\}$ represents the optimal long-term energy consumption of the entire system. With a similar approach, by allowing $\mathrm{N}\to\infty$, dividing both sides of inequality (66) by $\mathrm{N}V_L$, and disregarding certain non-negative terms, we can derive the following expression

$$\begin{aligned}
&\lim_{\mathrm{N}\to\infty}\frac{1}{\mathrm{N}}\sum_{n=0}^{\mathrm{N}-1}\mathbb{E}\Big\{\varepsilon e_u(n)+e_f(n)+\sum_{m\in\boldsymbol{M}}\Big\{e_m(n)+e_m^p(n)\Big\}\Big\}\\
&\le\frac{[F_{max}^u\delta_t]^2}{V_L\varphi^2}+e_u^{opt}(n)+\varepsilon e_f^{opt}+\sum_{m\in\boldsymbol{M}}\left\{e_m^{opt}+e_m^{p,opt}\right\}\\
&\triangleq\frac{[F_{max}^u\delta_t]^2}{V_L\varphi^2}+E^{opt}. \qquad (68)
\end{aligned}$$

This completes the proof of Theorem 1.

REFERENCES

[1] Y. Lin, W. Feng, Y. Wang, Y. Chen, Y. Zhu, X. Zhang, N. Ge, and Y. Gao, "Satellite-MEC integration for 6G internet of things: Minimal structures, advances, and prospects," *IEEE open J. Commun. Soc.*, vol. 5, pp. 3886-3903, Jun. 2024.

[2] H. Djigal, J. Xu, L. Liu, and Y. Zhang, "Machine and deep learning for resource allocation in multi-access edge computing: A survey," *IEEE Commun. Surv.*, vol. 24, no. 4, pp. 2449-2494, Aug. 2022.

[3] J. Huang, F. Liu, and J. Zhang, "Multi-dimensional QoS evaluation and optimization of mobile edge computing for IoT: A survey," *Chinese J. Electron.*, vol. 33, no. 4, pp. 859-874, Jul. 2024.

[4] Z. Han, T. Zhou, T. Xu, and H. Hu, "Joint user association and deployment optimization for delay-minimized UAV-aided MEC networks", *IEEE Wirel. Commun. Lett.*, vol. 12, no. 10, pp. 1791-1795, Oct. 2023.

[5] B. Liu, Y. Wan, F. Zhou, Q. Wu, and R. Q. Hu, "Resource allocation and trajectory design for MISO UAV-assisted MEC networks," *IEEE Trans. Veh. Technol.*, vol. 71, no. 5, pp. 4933-4948, May 2022.

[6] N. Kota and K. Naidu, "Minimizing energy consumption in H-NOMA based UAV-assisted MEC network," *IEEE Commun. Lett.*, vol. 27, no. 9, pp. 2536-2540, Sept. 2023.

[7] K. Xiang and Y. He, "UAV-assisted MEC system considering UAV trajectory and task offloading strategy," in *Proc. IEEE Int. Conf. Commun. (ICC)*, Rome, Italy, 2023, pp. 4677-4682.

[8] F. Pervez, A. Sultana, C. Yang, and L. Zhao, "Energy and latency efficient joint communication and computation optimization in a multi-UAV-assisted MEC network", *IEEE Trans. Wirel. Commun.*, vol. 23, no. 3, pp. 1728-1741, Mar. 2024.

[9] J. Zhu, X. Wang, H. Huang, S. Cheng, and M. Wu, "A NSGA-II algorithm for task scheduling in UAV-enabled MEC system," *IEEE Trans. Intell. Transp. Syst.*, vol. 23, no. 7, pp. 9414-9429, Jul. 2022.

[10] X. Zhang, L. Lv, L. Yang, X. Chu, A. Nallanathan, and J. Chen, "Hybrid NOMA offloading with semi-dynamic IRS beamforming in wireless powered MEC systems," *IEEE Wirel. Commun. Lett.*, vol. 13, no. 9, pp. 2447-2451, Sept. 2024.

[11] E. Michailidis, M. Volakaki, N. Miridakis, and D. Vouyioukas, "Optimization of secure computation efficiency in UAV-enabled RIS-assisted MEC-IoT networks with aerial and ground eavesdroppers," *IEEE Trans. Commun.*, vol. 72, no. 7, pp. 3994-4009, Jul. 2024.

[12] Y. Yang, Y. Hu, and M. C. Gursoy, "Energy efficiency of RIS-assisted NOMA-based MEC networks in the finite blocklength regime," *IEEE Trans. Commun.*, vol. 72, no. 4, pp. 2275-2291, Apr. 2024.

[13] J. Xu, A. Xu, L. Chen, Y. Chen, X. Liang, and B. Ai, "Deep reinforcement learning for RIS-aided secure mobile edge computing in industrial internet of things," *IEEE Trans. Industr. Inform.*, vol. 20, no. 2, pp. 2455-2464, Feb. 2024.

[14] C. Pan, G. Zhou, K. Zhi, S. Hong, T. Wu, and Y. Pan, "An overview of signal processing techniques for RIS/IRS-aided wireless systems," *J. Sel. Top. Signal Process*, vol. 16, no. 5, pp. 883-917, Aug. 2022.

[15] Y. Liao, J. Liu, X. Chen, Y. Han, Q. Ai, and G. Muntean, "Energy minimization of inland waterway USVs for IRS-assisted hybrid UAV-terrestrial MEC network," *IEEE Trans. Veh. Technol.*, vol. 73, no. 3, pp. 4121-4135, Mar. 2024.

[16] F. Jiang, Y. Peng, K. Wang, L. Dong, and K. Yang, "MARS: A DRL-based multi-task resource scheduling framework for UAV with IRS-assisted mobile edge computing system," *IEEE Trans. Cloud Comput.*, vol. 11, no. 4, pp. 3700-3712, Oct. 2023.

[17] M. Asim, M. ELAffendi, and A. El-Latif, "Multi-IRS and multi-UAV-assisted MEC system for 5G/6G networks: Efficient joint trajectory optimization and passive beamforming framework," *IEEE Trans. Intell. Transp. Syst.*, vol. 24, no. 4, pp. 4553-4564, Apr. 2023.

[18] Y. Gu, Y. Ma, X. Wang, and A. Shah, "Security energy efficiency optimization and analysis of aerial-IRS-assisted UAV-MEC system," *IEEE Access*, vol. 12, pp. 118953-118967, Aug. 2024.

[19] Y. Deng, H. Zhang, X. Chen, and Y. Fang, "UAV-assisted multi-access edge computing with altitude-dependent computing power," *IEEE Trans. Wirel. Commun.*, vol. 23, no. 8, pp. 9404-9418, Aug. 2024.

[20] X. Qin, Z. Song, T. Hou, W. Yu, J. Wang, and X. Sun, "Joint optimization of resource allocation, phase shift, and UAV trajectory for energy-efficient RIS-assisted UAV-enabled MEC systems," *IEEE Trans. Green Commun.*, vol. 7, no. 4, pp. 1778-1792, Dec. 2023.

[21] B. Duo, M. He, Q. Wu, and Z. Zhang, "Joint dual-UAV trajectory and RIS design for ARIS-assisted aerial computing in IoT," *IEEE Internet of Things J.*, vol. 10, no. 22, pp. 19584-19594, Nov. 2023.

[22] S. Wang, X. Song, T. Song, and Y. Yang, "Fairness-aware computation offloading with trajectory optimization and phase-shift design in RIS-assisted multi-UAV MEC network," *IEEE Internet of Things J.*, vol. 11, no. 11, pp. 20547-20561, Jun., 2024.

[23] P. Aung, L. Nguyen, Y. Tun, Z. Han, and C. S. Hong, "Aerial STAR-RIS empowered MEC: A DRL approach for energy minimization," *IEEE Wirel. Commun. Lett.*, vol. 13, no. 5, pp. 1409-1413, May 2024.

[24] H. Mei, K. Yang, J. Shen, and Q. Liu, "Joint trajectory-task-cache optimization with phase-shift design of RIS-assisted UAV for MEC," *IEEE Wirel. Commun. Lett.*, vol. 10, no. 7, pp. 1586-1590, Jul. 2021.

[25] Y. Liao, Y. Song, S. Xia, Y. Han, N. Xu, X. Zhai, and Z. Yuan, "Low-latency data computation of inland waterway USVs for RIS-assisted UAV MEC network," *IEEE Internet of Things J.*, vol. 11, no. 16, pp. 26713-26726, Aug. 2024.

[26] Y. Xu, T. Zhang, Y. Zou, and Y. Liu, "Reconfigurable intelligence surface aided UAV-MEC systems with NOMA," *IEEE Commun. Lett.*, vol. 26, no. 9, pp. 2121-2125, Sept. 2022.

[27] Y. Zeng, S. Chen, Y. Cui, and J. Du, "Efficient trajectory planning and dynamic resource allocation for UAV-enabled MEC system," *IEEE Commun. Lett.*, vol. 28, no. 3, pp. 597-601, Mar. 2024.

[28] F. Elghitani, "Dynamic UAV routing for multi-access edge computing," *IEEE Trans. Veh. Technol.*, vol. 73, no. 6, pp. 8878-8888, Jun. 2024.

[29] Y. Zeng, S. Chen, Y. Cui, J. Yang, and Y. Fu, "Joint resource allocation and trajectory optimization in UAV-enabled wirelessly powered MEC for large area," *IEEE Internet of Things J.*, vol. 10, no. 17, pp. 15705-15722, Sept. 2023.

[30] J. Zhang, L. Zhou, Q. Tang, E. Ngai, X. Hu, H. Zhao, and J. Wei, "Stochastic computation offloading and trajectory scheduling for UAV-assisted mobile edge computing", *IEEE Internet of Things J.*, vol. 6, no. 2, pp. 3688-3699, Apr. 2019.

[31] Z. Yang, S. Bi, and Y. Zhang, "Dynamic offloading and trajectory control for UAV-enabled mobile edge computing system with energy harvesting devices", *IEEE Trans. Wirel. Commun.*, vol. 21, no. 12, pp. 10515-10528, Dec. 2022.

[32] Z. Yang, S. Bi, and Y. Zhang, "Online trajectory and resource optimization for stochastic UAV-enabled MEC systems", *IEEE Trans. Wirel. Commun.*, vol. 21, no. 7, pp. 5629-5643, Jul. 2022.

[33] Z. Zhuo, S. Dong, H. Zheng, and Y. Zhang, "Method of minimizing energy consumption for RIS assisted UAV mobile edge computing system," *IEEE Access*, vol. 12, pp. 39678-39688, Mar. 2024.

[34] J. Zhang, L. Zhou, Q. Tang, E. Ngai, X. Hu, H. Zhao, and J. Wei, "Stochastic computation offloading and trajectory scheduling for UAV-assisted mobile edge computing", *IEEE Internet of Things J.*, vol. 6, no. 2, pp. 3688-3699, Apr. 2019.

[35] A. Hourani, S. Kandeepan, and A. Jamalipour, "Modeling air-to-ground path loss for low altitude platforms in urban environments", in *Proc. IEEE Global Telecommun. Conf. (GLOBECOM)*, Austin, TX, USA, 2014, pp. 2898–2904.

[36] A. Hourani, K. Sithamparanathan, and S. Lardner, "Optimal LAP altitude for maximum coverage", *IEEE Wirel. Commun. Lett.*, vol. 3, no. 6, pp. 569–572, Dec. 2014.

[37] Y. Cai, Z. Wei, S. Hu, C. Liu, D. Ng, and J. Yuan, "Resource allocation and 3D trajectory design for power-efficient IRS-assisted UAV-NOMA communications," *IEEE Trans. Wirel. Commun.*, vol. 21, no. 12, pp. 10315-10334, Dec. 2022.

[38] Y. Liao, Y. Song, L. Liu, and Y. Han, "Joint deployment and task scheduling in IRS-assisted wireless inland ship MEC network," in *Proc. IEEE Veh. Technol. Conf. (VTC)*, Florence, Italy, pp. 1-6, Aug. 2023.

[39] X. Zhang, J. Liu, R. Zhang, Y. Huang, J. Tong, N. Xin, L. Liu, and Z. Xiong, "Energy-efficient computation peer offloading in satellite edge

computing networks", *IEEE Trans. Mob. Comput.*, vol. 23, no. 4, pp. 3077-3091, Apr. 2024.
[40] J. Su, Z. Liu, Y. Xie, Y. Li, K. Ma, and X. Guan, "UEE-delay balanced online resource optimization for cooperative MEC-enabled task offloading in dynamic vehicular networks", *IEEE Internet of Things J.*, vol. 11, no. 7, pp. 11496-11507, Apr. 2024.
[41] T. Zhang and W. Chen, "Computation offloading in heterogeneous mobile edge computing with energy harvesting," *IEEE Trans. Green Commun.*, vol. 5, no. 1, pp. 552-565, Mar. 2021.
[42] R. Bi, Y. Sun, Y. He, T. Peng, M. Han, and G. Tan, "Utility-oriented computation scheduling for energy-efficient mobile edge computing networks," *IEEE Open J. Comput. Society*, vol. 3, pp. 260-270, Jan. 2022.
[43] S. M. Ross, *Introduction to Probability Models*. Amsterdam, The Netherlands: Academic, 2014.

Zheng Yao received the M.S. degree in control engineering from Chongqing University, Chongqing, China, in 2019, and the Ph.D. degree in control science and engineering from Wuhan University of Science and Technology, Wuhan, China, in 2023. He is currently a lecturer and master's supervisor of automation with the department of electrical and information engineering, Hubei University of Automotive Technology, Shiyan, China. His research interests include mobile edge computing, resource management, Lyapunov optimization theory, game theory, and their applications in wireless communications.

Qiwu Zhu received the B.Sc. degree in automation from Wuhan University of Science and Technology, Wuhan, China, in 2017, and the Ph.D. degree in software engineering from Chongqing University, Chongqing, China, in 2023. He is currently a postdoctoral fellow at The Hong Kong Polytechnic University, Hong Kong. His current research interests include wireless communication networks, internet of things, deep learning and intelligent systems.

Yanhui Zhang was born in Dongying, China, in 1984. He received Ph.D. degree in 2014 from University of Chinese Academy of Sciences. His main research interests include big data technology of new energy vehicles, power battery health assessment methods, fault diagnosis of electric vehicle batteries, safety guarantee of charging facilities.

Haibo Huang received the Ph.D. degree from Wuhan University, Wuhan, China, in 2011. He is currently a professor and master's supervisor of electronics with the department of electrical and information engineering, Hubei University of Automotive Technology, Shiyan, China. Currently, he holds the President of the School of Electrical and Information Engineering. His current research interests include automotive electronics and intelligent control. He participated as a key member in the research and development of the national defense "863" key project, and undertook five scientific research projects at the municipal level or above, including "Provincial Science and Technology Special Plan, Provincial Natural Science Foundation, and Provincial Education Department Key Project".

Min Luo received the M.S. degree in mechanical engineering from Chongqing University, Chongqing, China, in 1989. He is currently a researcher level senior Engineer, second level professor, master's supervisor of automation with the department of electrical and information engineering, Hubei University of Automotive Technology, Shiyan, China. His current research interests include numerical control technology and intelligent digital equipment. Currently, he holds the position of Director at the Automobile Intelligent Manufacturing Research Institute of Hubei Institute of Automotive Industry, in addition to being the Director of the Automobile Manufacturing Automation Branch at the National Engineering Research Center for Digitization of Manufacturing Equipment. His completed scientific research projects have garnered two Hubei Provincial Science and Technology Progress Awards, one China Automotive Industry Science and Technology Progress Award, two awards for scientific and technological progress from Shiyan City, and six Dongfeng Motor Technology Progress Awards.